

Anosmin-1 over-expression increases adult neurogenesis in the subventricular zone and neuroblast migration to the olfactory bulb

Diego García-González · Verónica Murcia-Belmonte · Pedro F. Esteban · Felipe Ortega · David Díaz · Irene Sánchez-Vera · Rafael Lebrón-Galán · Laura Escobar-Castañondo · Luis Martínez-Millán · Eduardo Weruaga · José Manuel García-Verdugo · Benedikt Berninger · Fernando de Castro

Received: 27 January 2014 / Accepted: 23 September 2014 / Published online: 10 October 2014
© Springer-Verlag Berlin Heidelberg 2014

Abstract New subventricular zone (SVZ)-derived neuroblasts that migrate via the rostral migratory stream are continuously added to the olfactory bulb (OB) of the adult rodent brain. Anosmin-1 (A1) is an extracellular matrix protein that binds to FGF receptor 1 (FGFR1) to exert its biological effects. When mutated as in Kallmann syndrome patients, A1 is associated with severe OB morphogenesis defects leading to anosmia and hypogonadotropic hypogonadism. Here, we show that A1 over-expression in adult mice strongly increases proliferation in the SVZ, mainly with symmetrical divisions, and produces substantial morphological changes in the normal SVZ architecture, where we also report the presence of FGFR1 in almost all

SVZ cells. Interestingly, for the first time we show FGFR1 expression in the basal body of primary cilia in neural progenitor cells. Additionally, we have found that A1 over-expression also enhances neuroblast motility, mainly through FGFR1 activity. Together, these changes lead to a selective increase in several GABAergic interneuron populations in different OB layers. These specific alterations in the OB would be sufficient to disrupt the normal processing of sensory information and consequently alter olfactory memory. In summary, this work shows that FGFR1-mediated A1 activity plays a crucial role in the continuous remodelling of the adult OB

Keywords Neural stem cell · Interneuron · Cell migration · FGF2 · Primary cilium · GnRH neuron · Kallmann syndrome

F. Ortega, D. Díaz and I. Sánchez-Vera contributed equally.

Electronic supplementary material The online version of this article (doi:10.1007/s00429-014-0904-8) contains supplementary material, which is available to authorized users.

D. García-González · V. Murcia-Belmonte · P. F. Esteban · R. Lebrón-Galán · F. de Castro (✉)
Grupo de Neurobiología del Desarrollo-GNDe,
Hospital Nacional de Paraplégicos, Toledo, Spain
e-mail: fdec@sescam.jccm.es

Present Address:
D. García-González
Clinical Neurobiology, German Center for Cancer
Research (DKFZ), Heidelberg, Germany

Present Address:
V. Murcia-Belmonte
Instituto de Neurociencias, Universidad Miguel
Hernández-CSIC, Alicante, Spain

F. Ortega · B. Berninger
University Medical Center Johannes Gutenberg,
University of Mainz, Mainz, Germany

D. Díaz · E. Weruaga
Instituto de Neurociencias de Castilla y León-INCyL,
Universidad de Salamanca, Salamanca, Spain

I. Sánchez-Vera · J. M. García-Verdugo
Laboratorio de Neurobiología Comparada, Instituto Cavanilles,
Universidad de Valencia, CIBERNED, Valencia, Spain

I. Sánchez-Vera
Unidad mixta de Esclerosis múltiple y neuroregeneración,
IIS Hospital La Fe, Valencia, Spain

L. Escobar-Castañondo · L. Martínez-Millán
Departamento de Neurociencias, Facultad de Medicina,
Universidad del País Vasco, Leioa, Spain

Introduction

Olfactory perception plays an important role in the relationship of the majority of vertebrates with the external world. In the adult rodent brain, the olfactory bulb (OB) continuously receives newly generated neurons (Álvarez-Buylla and Lim 2004). These newborn cells reach the OB following a long migratory pathway called the rostral migratory stream (RMS). The site of origin of these migrating neuroblasts is the subventricular zone (SVZ), an extensive germinal niche adjacent to the walls of the lateral ventricles. In the SVZ, primary progenitors give rise to transit-amplifying precursor cells, which expand the population and in turn differentiate into neuroblasts and oligodendrocytes (Lois and Álvarez-Buylla 1994; Doetsch et al. 1999, 2002; Aguirre and Gallo 2004; Menn et al. 2006). Neurogenesis is modulated by numerous extrinsic factors, including extracellular matrix (ECM) molecules, morphogens, growth factors and neurotransmitters (for a detailed review: Ihrle and Álvarez-Buylla 2011).

Extracellular matrix molecules are secreted into the extracellular space, where they associate with cell surface receptors and regulate diverse cell functions, such as migration and differentiation (Shen et al. 2008; Raymond et al. 2009; Pujadas et al. 2010). Anosmin-1 (A1) is an ECM protein encoded by the *KALI* gene in humans (Franco et al. 1991; Legouis et al. 1991). A1 can interact with other ECM proteins (laminin, fibronectin, and even A1 itself), heparan sulphate proteoglycans and the FGF receptor 1 (FGFR1), being this latter the most studied to date (Bülow et al. 2002; González-Martínez et al. 2004; Hu et al. 2004, 2009; Murcia-Belmonte et al. 2010; Esteban et al. 2013). Mutations in the *KALI* and *FGFR1* genes give rise to Kallmann syndrome (KS), a disease accompanied by hypogonadotropic hypogonadism and anosmia, generally caused by a disrupted OB morphogenesis (Maestre de San Juan 1856; Kallmann et al. 1944; Franco et al. 1991; Legouis et al. 1991; Dodé et al. 2003). The study of A1 expression pattern in the postnatal rat brain reveals a prominent presence of this molecule in the olfactory system, with high expression levels in OB mitral cells and interneurons (Clemente et al. 2008). A1 promotes the FGFR1-mediated migration of gonadotropin releasing hormone-derived neurons and SVZ neuroblasts (Cariboni et al. 2004; García-González et al. 2010). Additionally, A1 intervenes in the migration of oligodendrocyte precursor cells with a FGFR1-mediated effect (Bribián et al. 2006, 2008; Clemente et al. 2008; Murcia-Belmonte et al. 2014).

Most studies on A1 functions in the central nervous system (CNS) were based on different gain- and loss-of-function approaches in diverse experimental models

(Bülow et al. 2002; Rugarli et al. 2002; Andrenacci et al. 2006; Yanicostas et al. 2009). Despite its highly conserved sequence across species, including some rodents (i.e., the guinea pig and the squirrel) the orthologue in mice and rats has not been found yet. In consequence, a mouse model is still unavailable and hampers a deeper understanding of A1 functions in rodents. As clearly indicated by the literature on A1 and KS, A1 functions affect multiple cell types and systems (Soussi-Yanicostas et al. 2002; Cariboni et al. 2004; Bribián et al. 2006; Gianola et al. 2009; García-González et al. 2010; Murcia-Belmonte et al. 2010; Clemente et al. 2011; Esteban et al. 2013). Based on functional results obtained in transgenic mice over-expressing the human *KALI* cDNA, in this study, we investigated the role of A1 in adult SVZ neurogenesis and migration to the OB. In A1 over-expressing mice, we discovered increased proliferation rates in the SVZ that, together with enhanced neuroblast motility, led to alterations in the density of specific OB interneuron populations. Moreover, A1 over-expression caused changes in the SVZ morphology, especially in FGFR1-expressing cells. The phenotype observed highlights the importance of the complex A1-FGFR1 to key biological processes such as neurogenesis and cell migration.

Materials and methods

Generation of transgenic mice over-expressing anosmin-1

The human *KALI* cDNA was used to generate a transgenic mouse line that over-expresses A1 under the control of the human β -actin promoter carried by the pBAP vector (Gunning et al. 1987), kindly provided by Dr. Lino Tesarollo (NCI, Frederick, MD 21702, USA), followed by an IRES sequence and the EGFP cDNA as a reporter. The EGFP facilitated detection in mice by Western blot. DNA injection and generation of founders was carried out at the *Unidad de Generación de Organismos Modificados Genéticamente, Servicio de Experimentación Animal de la Universidad de Salamanca*, Spain. Genotyping PCR strategies were performed on tail genomic DNA using the following primers:

hKalexon11: 5'-GGTACTGTCCAACCAATACG-3';
 hKalexon12: 5'-GGAAGGCAGAATCTGGGACTG-3';
 EGFP15: 5'GCGACGTAAACGGCCACAAG-3';
 EGFP23: 5'-CGGTCACGAACCTCCAGCAGG-3'.

The expression pattern of GFP in the transgenic line was examined by GFP Western blotting. All the experiments using animals were in accordance with Spanish (RD 53/2013) and European Communities Council Directive

(2013/63/UE) regulation and they were approved by the animal review board at the Hospital Nacional de Paraplégicos (registered as SAPA001).

Histological procedures

C57BL/6 wild-type (+/+) and A1 over-expressing transgenic 10–12 week-old mice were deeply anaesthetised, then intracardially perfused with 4 % paraformaldehyde (PFA) in 0.1 M, pH 7.4 phosphate buffer (PB), postfixed in the same fixative for 4 h and washed in PB three times. Brains were cryoprotected in 30 % (w/v) sucrose in PB and frozen by immersion in pre-cooled isopentane. Coronal (20 or 70 μm thick) or sagittal sections (60 μm thick) were obtained with a cryostat (Leica) or microtome (Leica) and stored at $-20\text{ }^{\circ}\text{C}$ until used. After several washes in PB, sections were blocked in PBS with 5 % normal donkey or goat serum (Vector Laboratories) and permeabilised in PBS with 0.2 or 0.5 % Triton X-100 for 1 h at room temperature (RT). The following primary antibodies were used: rabbit anti-Olig2 (1:200; Millipore AB9610), rabbit anti-parvalbumin (PV; 1:1,000; Swant PV235), rabbit anti-calretinin (CR; 1:5,000; Swant 7699/3H), rabbit anti-calbindin (CB; 1:15,000; Swant CB-38a), sheep anti-tyrosine hydroxylase (TH; 1:1,000; Millipore AB1542), mouse anti-Mash1 (courtesy of Dr. Vicario-Abejón), mouse anti-NeuN (1:100; Millipore MAB377), rat anti-BrdU (1:200; Acris SM1667PS), rabbit anti-phospho Histone H3 (PH3; 1:200; Abcam ab5176), rabbit anti-cleaved caspase-3 (1:1,000; RD MAB835), rabbit anti-FGFR1 (1:200; Cell Signalling), mouse anti-nestin (1:500; BD 556309), goat anti-vimentin (1:500; Santa Cruz sc-7557), goat anti-doublecortin (DCX; 1:200; Santa Cruz sc-8066), mouse anti- β III tubulin (clone Tuj1; 1:1,000; Millipore MAB5564) and rabbit anti-GFAP (1:500, DAKO Z0334).

For immunohistochemistry, the peroxidase method with biotinylated secondary antibodies (all of them 1:200; Vector Laboratories) with the standard ABC Elite reagent (Vector Laboratories), 0.0125 % DAB (diaminobenzidine; Sigma-Aldrich) as chromogen and 0.003 % H_2O_2 in 0.1 M Tris-HCl, pH 7.6 was performed. Nickel ammonium sulphate was added to the solution in some cases to increase the contrast. Tissue from animals of the same age was developed with DAB in the same staining tank and the same reaction time was applied to all the samples in the tank. Counterstained cell profiles were visualised with Nissl and toluidine blue.

For immunofluorescence, Alexa 488, Alexa 594, Alexa 647 (1:1,000, Invitrogen) secondary antibodies were used. Cells were stained with Hoechst 33342 to visualise nuclei (10 $\mu\text{g}/\text{mL}$; Sigma-Aldrich). Fluorescent sections were mounted on slides with Fluoromount G (SouthernBiotech) and a coverslip. Images were captured with a confocal

microscope TCS SP5 (Leica) or TCS resonant scanner (Leica) as appropriate.

BrdU injections

Adult animals (P60; wild-type $n = 5$; A1 over-expressing mice $n = 3$) received four injections of BrdU intraperitoneally every 2 h in 1 day (50 mg/kg body weight, 10 mg/mL; Sigma-Aldrich). For all experimental groups, mice were killed 20 days after the last injection and then brains were collected and processed for histology, as described above.

Stereological quantifications

The use of the stereological approach produced data containing consistent cell counts with variances within each sample and across sampling sites that were in a statistically acceptable range. Using stereology to comprehensively analyse brain regions of interest eliminates bias selecting sites to evaluate and chance differences (Peterson 1999).

Volume estimation

The total volume of the OB and each of its layers were estimated ($n = 10$ wild-type and $n = 6$ A1 over-expressing mice) using the NewCAST Grid software and the principle of Cavalieri (1966).

Cell counting

Unbiased estimations of the density of NeuN ($n = 6$ mice/group), CR ($n = 6$ /group), CB ($n = 8$ /group), TH ($n = 3$ /group), and PV ($n = 3$ /group) immunopositive cells were performed using an optical dissector unbiased sample design (Gundersen et al. 1988). Stereological analysis was performed with an Olympus BX51 microscope with a calibrated motorised stage controller that allows precise control of x -, y - and z -axes linked to the New CAST software. Each corresponding layer (granule, GR; external plexiform, EPL; glomerular, GL) was outlined using a $2\times$ objective on each of the toluidine blue stained coronal sections (70 μm thick). Series of six sections of OB, regularly spaced at intervals of 420 μm and covering the entire OB, were used for cell counting. From a random start position, a counting frame was superimposed on the image and neurons were sampled using a $100\times$ objective. Immunopositive cells were included when the soma came into focus and did not touch the exclusion lines of the counting frame. A sampling frame size of $1,204.7\ \mu\text{m}^2$ was used and each one was spaced every 352.18 or 248.03 μm along the x and y axis from each other, depending on the region shape. The dissector z -step was 15 μm and a guard zone of 4 μm at both the upper and the lower surface of the section

was used. A minimum of 200 cells were sampled according to the rules of the optical dissector method.

BrdU⁺ cell density in the whole OB was similarly estimated in parasagittal sections 60 µm thick using the optical dissector method (sampling frame size 1,204.7 µm², frame step 352.18 µm, dissector z-step 15 µm) to evaluate the relative number of cells that reached the OB from the SVZ 20 days after the injections, assuming that the vast majority of them are newborn neurons (Petreanu and Álvarez-Buylla 2002).

Other cell counting

To evaluate densities of cleaved caspase-3⁺, PH3⁺ and PH3⁺/DCX⁺ cells within each region of interest, a blind method of counting cells within standardised regions of SVZ ($n = 3$ mice/group) was adopted. For all the counts, four 40× z-stack images obtained dorso-ventrally on a confocal SP5 resonant microscope (Leica) were examined in five representative antero-posterior sections (20 µm thick) in each brain. In addition, the relative number of mitral cells was estimated following the same standardised system.

Cell cultures

Chemotaxis assays

SVZs of P0 mice were dissected and then dissociated in DMEM (Invitrogen) containing 0.025 % Trypsin (at 37 °C, for 30 min), and 0.05 % DNase was added for 5 min. Trypsin was blocked by adding 10 % foetal bovine serum (FBS) and the cells were collected by centrifugation (150×g; 5 min). In each Boyden chamber (8 µm pore, 12 mm diameter; Corning Costar Corp.) 40,000 cells were seeded in the upper compartment in culture medium composed by DMEM-F12 (Invitrogen) complemented with 5 % FBS, 5 % horse serum (HS) and 1 % v/v P-S (Invitrogen), whilst in the lower compartment culture medium was supplemented for the different experimental groups as follows: (a) CHO-CT concentrated ECM extract or (b) CHO-A1 concentrated ECM extract. These CHO lines, CHO wild-type control cells (CHO-CT) and CHO cells expressing the C-terminal HA-tagged full-length anosmin-1 (see above CHO-A1), were used to prepare ECM protein extracts following a modified protocol described before (Soussi-Yanicostas et al. 1996). Briefly, cells were washed once with calcium/magnesium-free Hank's Balanced Salt Solution and then incubated with gentle rocking for 30 min at 4 °C in 1 mL per culture dish (10 cm in diameter) of 20 mM phosphate buffer pH 7.4, containing 350 mM NaCl and complete EDTA-free protease inhibitor (Roche). ECM proteins released into the buffer were concentrated ten

times using Amicon Ultra-4 Ultracel-30k (Millipore). Additionally, SVZ-derived cells were treated during the experiment with the FGFR-specific inhibitor SU5042 (10 µM; Calbiochem-Merck) where indicated, and the rest of the cultures were exposed to an equal volume of the vehicle DMSO (Sigma-Aldrich). After 20 h, cultures were fixed with 4 % PFA (for 10 min, at RT) and the presence of neuroblasts in the lower chamber was evaluated using Tuj1 Ab (1:1,000, Millipore MAB5564), whilst nuclei were stained with Hoechst 33342 (10 µg/mL; Sigma-Aldrich). Appropriate fluorescence-labelled secondary antibodies were used in each case. After immunostaining, the Boyden filters were examined with an In Cell 1000 Analyzer (software In Cell 1000 Analyzer; GE-HealthCare) and 16 microphotographs from each membrane were taken randomly in 4 independent experiments per genotype. To quantify chemotropism, the number of transmigrated neuroblasts per field was counted using the software In Cell 1000 Analyzer Workstation (GE-HealthCare). The data were expressed as percentage of migrating neuroblasts relative to control conditions ± SEM, considered as 100 % (García-González et al. 2010; Murcia-Belmonte et al. 2010; Esteban et al. 2013).

Culture of SVZ explants and video time-lapse (VTL) tracking for migration

Brains were dissected out from newborn P0 mice. Coronal sections of 350 µm in thickness were obtained with a tissue chopper (McIlwain) and the SVZ was carefully dissected with microneedles. Explants were embedded in rat tail collagen (1:1) as described previously (García-González et al. 2010), and they were cultured at 37 °C in 5 % CO₂ and at 95 % humidity for 3 days in vitro (3 DIV) in DMEM-F12 (1:1; Invitrogen) medium complemented with 5 % FBS, 5 % HS and 1 % v/v P-S, without any supplementary cue to test the intrinsic motility of neuroblasts for each animal group (wild-type and A1). After 3 DIV, explants were fixed with 4 % PFA before immunolabelling with Tuj1 (1:1,000, Millipore MAB5564), DCX (1:200, Santa Cruz sc-8066), GFAP (1:500, Dako Z0334) or Olig2 (1:200, Millipore AB9610). Nuclei were stained with Hoechst 33342 (10 µg/mL; Sigma-Aldrich). Surfaces occupied by migrating cells and explants were estimated using the ImageJ software (National Institutes of Health). Four independent experiments were performed for each condition and 59 and 64 explants from wild-type and A1 over-expressing mice, respectively, were evaluated.

Images for the VTL tracking were taken every 20 min over the first 48 h of the experiment, using phase-contrast microscopy (Olympus IX81), digitalised and analysed using image-processing software (Cell-R, Olympus and ImageJ). The total migrated distance was calculated as the sum of all

the partial trajectories travelled by a cell every 20 min; when the migrated distance was zero, it was defined as a stop. The migration speed was also calculated. Two independent cell tracking experiments were carried out and 12 explants were analysed per condition and experiment. Finally, 277 and 386 cells from wild-type and transgenic mice, respectively, were studied for quantifications.

Dissociated cell cultures for cell proliferation and lineage analysis

SVZ cultures were prepared from the lateral and dorsal wall of the adult SVZ of young adult (8–12 weeks) wild-type or A1 over-expressing mice. Briefly, the tissue was enzymatically dissociated in 0.7 mg/mL hyaluronic acid (Sigma-Aldrich) and 1.33 mg/mL trypsin (Sigma-Aldrich) in Hanks' Balanced Salt Solution (HBSS; Invitrogen) with 2 mM glucose at 37 °C for 30 min. Dissociation was stopped by adding an equal volume of ice-cold medium consisting of 4 % bovine serum albumin (BSA; Sigma-Aldrich) in Earle's Balanced Salt Solution (EBSS; Invitrogen), buffered with 20 mM HEPES (Invitrogen). Cells were then centrifuged at 270×g for 5 min, re-suspended in ice-cold medium consisting of 0.9 M sucrose (Sigma-Aldrich) in 0.5× HBSS, and centrifuged for 10 min at 650×g. The cell pellet was re-suspended in 2 mL ice-cold medium consisting of 4 % BSA in EBSS buffered with 2 mM HEPES, and the cell suspension was placed on top of 12 mL of the same medium and centrifuged for 7 min at 300×g. The cell pellet was finally re-suspended in DMEM/F12 (Invitrogen) supplemented with B27 (Invitrogen), 2 mM glutamine (Sigma-Aldrich), 100 units/mL penicillin (Invitrogen), 100 µg/mL streptomycin (Invitrogen), buffered with 8 mM HEPES, and cells were plated on poly-L-lysine (Sigma-Aldrich) coated coverslips at a density of 200–300 cells per mm².

After 6 DIV cultures were fixed in 4 % PFA in PBS for 15 min at room temperature and processed for antibody staining. Antibodies used were: mouse IgG2b anti-βIII tubulin (Sigma-Aldrich; 1:1,000), mouse IgG1 anti-GFAP (Sigma-Aldrich; 1:500). Secondary antibodies were chosen according to the primary antibodies and were coupled to Alexa488 or FITC, Cy3, Alexa647, Cy5 or biotinylated secondary antibodies and nuclei were counterstained with DAPI (Sigma-Aldrich).

Video time-lapse microscopy for cell proliferation and lineage analysis

Time-lapse video microscopy and single-cell tracking (Ortega et al. 2011) of primary SVZ cultures was performed with a cell observer (Zeiss) at a constant

temperature of 37 °C and 8 % CO₂. Phase-contrast images were acquired every 5 min for 6–10 days using a 20× phase-contrast objective (Zeiss), an AxioCam HRm camera and a Zeiss AxioVision 4.7 software. Neurogenic nature of the cells generated was confirmed by post-imaging immunocytochemistry. Single-cell tracking was performed using a self-written computer program (TTT) (Rieger et al. 2009).

Dissociated cell cultures for cell proliferation

We analysed BrdU incorporation into SVZ-derived cells from P1 to P3 pups as described previously (García-González et al. 2010). After 42 h in culture, BrdU (50 µM) was added to the culture medium for 6 h and then, the culture medium was refreshed for the last 24 h of the experiment. The incorporation of BrdU was detected with a BrdU antibody (1:500; Acris SM1667PS) and BrdU+ cells were classified with Tuj1 (1:1,000; Millipore MAB5564), nestin (1:500; BD 556309) and GFAP (1:500; Dako Z0334). Primary antibodies were detected with Alexa 488, Alexa 594, Alexa 647 (1:1,000, Invitrogen) secondary antibodies and nuclei were stained with Hoechst 33342 (10 µg/mL; Sigma-Aldrich). Cells were treated during the experiment with FGFR-specific inhibitor SU5042 (10 µM; Calbiochem-Merck) where indicated. Control cultures were exposed to an equal volume of the vehicle DMSO (Sigma).

Quantitative real-time PCR analysis

For RNA purification from brain tissues, animals were anaesthetised and decapitated. Olfactory bulbs from three animals per genotype were immediately removed, rapidly frozen in dry ice and stored at –80 °C before processing with Trizol[®] (Invitrogen) and retro-transcribed into cDNA using the High Capacity cDNA Reverse Transcription kit (Applied Biosystems), as previously described (García-González et al. 2010). We performed quantitative real-time PCR (qRT-PCR) assays for *KALI*, *th* and *gapdh* mRNAs using the corresponding TaqMan probes and oligonucleotides (*KALI*, Hs00608006_m1*, *th*, Mm00447557_m1* and mouse *Gapdh* as endogenous control, Mm99999915_g1*). Reactions were developed in an ABI PRISM[®] 7900HT Sequence Detection System (Applied Biosystems) in 96-well plates. Relative quantification was determined using the comparative Ct method as described in the ABI PRISM user manual and at least three replicates per sample were performed. Relative *KALI* expression was normalised to the lowest expressing littermate and averaged for A1 transgenic mice. Expression results for the each TaqMan probe were calculated normalising to the wild-type animal.

Electron microscopy

Three adult mice per genotype (80 days old) were deeply anaesthetised and perfused transcardially with 0.9 % PBS followed by 100 mL of Karnovsky's fixative (2 % PFA, 2.5 % glutaraldehyde) for conventional EM. Brains were postfixed with the same fixative overnight at 4 °C. Two hundred micrometer sections were postfixed in 2 % osmium for 1.5 h, rinsed, dehydrated, and embedded in Araldite (Sigma-Aldrich). Serial 1.5- μ m semithin sections were stained with 1 % toluidine blue and examined under a light microscope to study the overall organisation of the SVZ. Finally, ultra-thin sections (60–80 nm) were cut with a diamond knife, stained with lead citrate (Reynolds solution) and examined under a FEI Tecnai G2 Spirit transmission electron microscope (FEI Europe, Eindhoven, The Netherlands) using a digital camera (Morada, Olympus Soft Image Solutions GmbH). Adjustment of brightness and contrast of the pictures, if needed, was performed with Adobe Photoshop CS (Adobe Systems).

Whole-mount dissection, immunostaining and microscopy

After cervical dislocation of P80 mice, hemispheres were freshly extracted and separated in L15 at 4 °C. The hippocampus and septum were removed from the caudal aspect of the telencephalon and the walls of the lateral ventricles were fixed by immersion in 4 % PFA–0.1 % Triton X-100 overnight at 4 °C. After staining, the ventricular walls were further dissected from the underlying parenchyma as slices of tissue 200–300- μ m thick and were mounted on slides with Fluoromount G (SouthernBiotech) and a coverslip (for further details see: Mirzadeh et al. 2010a). Four animals per group were analysed.

Primary and secondary antibodies were incubated in PBS with 1 % Triton X-100 and 10 % normal goat or donkey serum for 24 h at 4 °C. Mouse anti-acetylated tubulin antibody was used to stain the whole cilium (1:1,000, Sigma-Aldrich T6793). Secondary antibodies conjugated to Alexa 488, Alexa 594, Alexa 647 (1:500, Invitrogen) were also used. Confocal images were taken on a TCS SP5 resonant scanner (Leica).

Tracer injections and study of the lateral olfactory tract

Axon efferents from the OB were labelled with the tracer biotindextranamine (BDA) 10000 (Sigma-Aldrich). Animals were anaesthetised with an intra-muscular (i.m.) injection of a mixture of ketamine chlorhydrate (36 mg/kg body weight; Sigma-Aldrich) and xylazine (6.2 mg/kg body weight; Rompun, Bayer). With a 35G needle and a nanofil syringe (World Precision Instruments) 1.5 μ L of a

10 % BDA solution in distilled water was injected (0.15 μ L/min). The tip of the needle was placed 2 mm before the frontoparietal suture, 1 mm lateral to the middle line and 1.5 mm below the piamater. Prophylactic antibiotics were administered preoperatively (chloramphenicol, 30 mg/kg i.m.) and postoperatively (gentamycin, 40 mg/kg i.m.). Postoperative pain was managed with buprenorphine (0.03 mg/kg i.m.) for 3 days. 7–10 days postsurgery, animals were anaesthetised and perfused transcardially as explained above. From each telencephalon, series of 60 μ m cryostat coronal sections were collected and treated for 20 min with 1 % H₂O₂ in PBS and then incubated overnight at 4 °C with 1:200 avidin–biotinperoxidase (Vectastain kit, Vector Laboratories) in PBS containing 0.5 % Triton X-100. The reaction product was developed in 0.02 % DAB and 0.02 % H₂O₂ in 50 mM Tris–HCl, pH 7.6. Sections were mounted on gelatine-coated slides, dehydrated in ethanol, cleared in xylene, and coverslipped with DPX mounting medium (Fluka Química).

Behavioural tests

Olfactometry

Mice were trained in custom-built computer-controlled six-channel air-dilution olfactometers (<http://www.olfactometer.com>; Lazarini et al. 2009; Díaz et al. 2012). Briefly, electronic valves controlled purified air streams, passing over the surface of mineral oil-diluted odorants. This odorized air was diluted 1:40 in odour-free air before its introduction into an odour sampling tube in the mouse operant chamber. The odorants used were (+)-carvone and (–)-carvone (99 %; Sigma-Aldrich). Partially water-deprived mice (80–85 % of their baseline body weight) were trained using an operant conditioning go/no-go paradigm. Standard operant conditioning methods were used to train mice to insert their snouts into the odour sampling port for at least 1.2 s and to respond by licking the water delivery tube (within the same port) to get a water reward (3 μ L) in the presence of a positive odour stimuli, (+)-carvone (reinforced stimulus: S+), and to refrain from licking and retract their head from the sampling port in the presence of a negative odour stimulus (unreinforced stimulus: S–). In each trial, a single stimulus was presented and S+ and S– trials were presented in a modified random order. The percentage of appropriate responses was determined for each block of 20 trials. A score of ≥ 85 % implied that mice had correctly learnt to assign reward/non-reward values. Each mouse underwent a session of 10 blocks (200 trials) per day. Mice were first trained with (+)-carvone versus mineral oil, reaching a plateau of performance after 30 blocks. Decreasing concentrations of odorant were used to determine their odour detection

threshold: $[10^{-2}]$, $[10^{-3}]$, $[10^{-4}]$ and $[10^{-5}]$. For odour discrimination tests, two odorants were used: (+)-carvone as S+ and (–)-carvone as S–, both diluted to $[10^{-2}]$. After discrimination of the pure odorant molecules (100-0), we tested odour discrimination threshold by gradually presenting binary odour mixtures of those carvone enantiomers: 80-20 (80 % (+)-carvone/20 % (–)-carvone for S+, and 80 % (–)-carvone/20 % (+)-carvone the S–), 68-32, and 56-44.

Short-term olfactory memory

Animals were exposed to odorants by placing in a 5×5 cm plastic dish a 2×2 cm Whatman filter paper impregnated with 10 μ L of a 0.4 % solution of the corresponding odorant in odourless mineral oil (all reactivities were obtained from Sigma-Aldrich). Two days before the experiment, animals underwent one familiarisation session with the cage and the procedure by exposing them to mineral oil. The mouse was placed in the test cage for 10 min and exposed to mineral oil for 2 min before each session, each one consisting of two consecutive exposures to mint odorant (5 min each), with two different intervals (15 and 30 min) between both exposures. The time spent investigating the odorant was recorded for each animal.

Quantitative and statistic analysis

The data are presented as the mean \pm SEM. These data have been compared in accordance with Student's *t* test or two-way ANOVA. Statistical analysis of the quantitative results was conducted using the Sigmastat software package (SPSS Inc.). Data were analysed by unpaired or paired Student's *t* tests, when appropriate.

Results

Generation of anosmin-1 transgenic mice

We generated transgenic A1 over-expressing mice, by placing the full-length human *KALI* cDNA under the control of the β -actin promoter followed by an IRES sequence and the EGFP cDNA (Fig. 1a). The transgenic mice were viable, fertile and transmitted the transgene. EGFP and *KALI* insertion were confirmed by PCR genotyping on tail genomic DNA (Fig. 1b). To confirm the expression of the human *KALI* mRNA in transgenic mice, we carried out quantitative real-time PCR using cDNA amplified from brain mRNA, with a specific human *KALI* Taqman Probe (Fig. 1c). The results confirmed that the transgenic mice expressed the human *KALI* cDNA. GFP

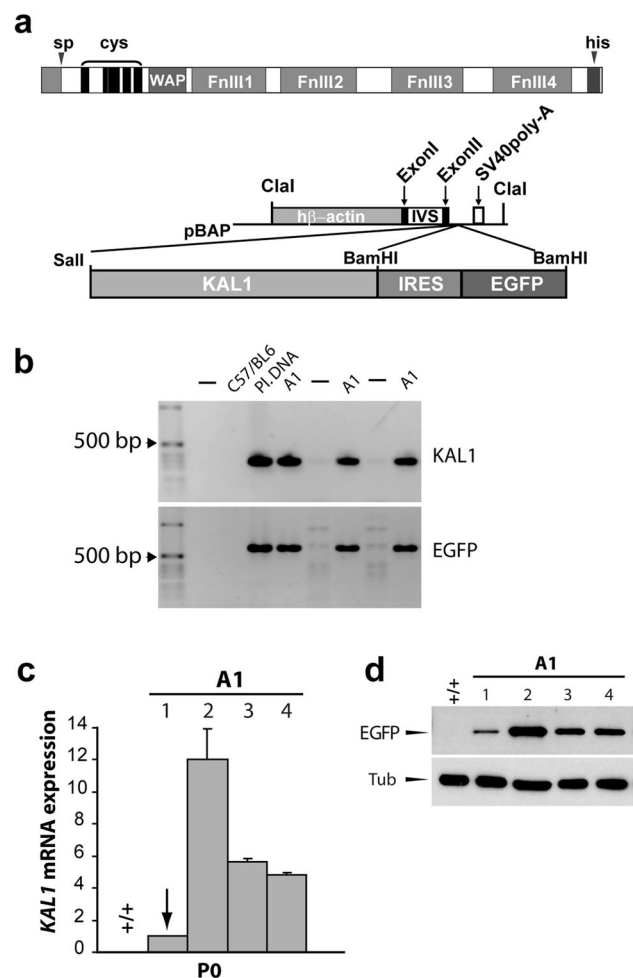


Fig. 1 Initial characterisation of A1 over-expressing transgenic mice. **a** Scheme representing the A1 structure and the transgene generated. A human *KALI* cDNA was used to generate a transgenic line that over-expresses anosmin-1 under the control of the promoter of the human β -actin gene carried by the pBAP vector. **b** The inserted cassette was detected in transgenic mice by PCR of *KALI* and EGFP cDNA. **c** *KALI* mRNA expression levels were evaluated by RT-PCR in P0 mice. **d** The *KALI* RNA expression was also confirmed by western blot

expression by Western blot paralleled the *KALI* mRNA expression (Fig. 1d). After back-crossing four times to C57BL/6 mice, the transgene expression was found to be stable and a line expressing a high level of *KALI* mRNA compared to the rest of the lines, was used to continue the back-crossing and to generate by intercrossing the transgenic line (Fig. 1d).

Anosmin-1 over-expression impairs olfactory short-term memory without affecting perception and discrimination

Since A1 has extensively been linked to olfactory deficits in KS patients, we investigated the olfactory behaviour of

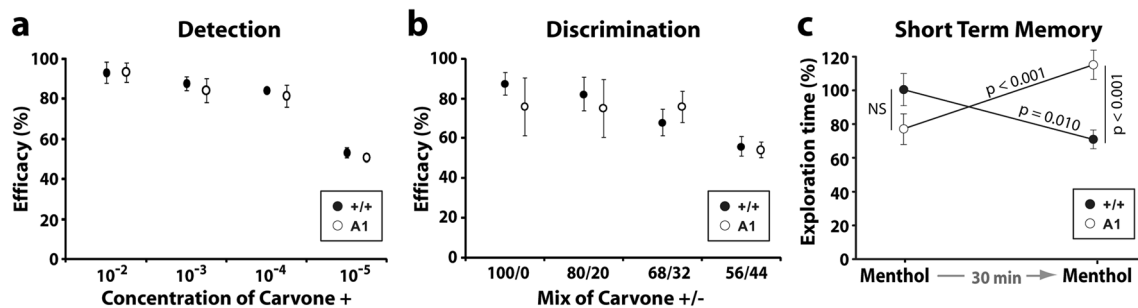


Fig. 2 Anosmin-1 over-expression impairs short-term olfactory memory without affecting olfactory detection or discrimination. **a** Control and A1 mice exhibited a similar performance detecting decreasing concentrations of (+)-carvone (wild-type $n = 4$; A1 $n = 6$). **b** Discrimination levels between different mixtures of enantiomers (+)-carvone/(−)-carvone was not affected (wild-type $n = 4$; A1 $n = 6$) in A1 over-expressing mice. **c** Short-term memory was impaired in A1 over-expressing animals since after 30 min of

interval, wild-type mice significantly spent less time sniffing menthol (0.4 %) than in the first exposure (Student's paired t test; $t_{(16)} = 2.907$, $p = 0.010$), whilst A1 over-expressing mice increased their exploration time compared with the first exposure (Student's paired t test; $t_{(17)} = -4.469$, $p < 0.001$), spending significantly more time than wild-type mice in the second exposure (Student's t test; $t_{(33)} = -3.818$, $p < 0.001$) (wild-type $n = 17$; A1 $n = 18$). Data are presented as mean \pm SEM

A1 over-expressing mice. Animals were first trained to associate the odour (+)-carvone (S+) with a reward and to retract their head from the odour sampling port in the presence of the odourless mineral oil (S−). To establish a detection threshold, animals were exposed to (+)-carvone over a range of concentrations. When starting at an odour concentration of 10^{-2} , all mice reached the 85 % performance criterion, demonstrating a normal capacity to detect high concentration odorants ($t_{(8)} = 0.330$, $p = 0.890$; Fig. 2a). Similarly, wild-type and A1 over-expressing mice showed a similar performance according to progressively decreasing concentrations (10^{-3} , 10^{-4} and 10^{-5}).

Subsequently, we investigated the capacity of mice to discriminate between monomolecular enantiomers: (+)-carvone versus (−)-carvone. When starting from pure molecules (100 %) at a dilution of 10^{-2} (defined as an easy task), all mice reached the performance criterion of 85 % of correct choices ($t_{(8)} = 1.506$, $p = 0.121$; Fig. 2b). When using binary mixtures, thus increasing the complexity of the task (80/20 %, 68/32 % and 56/44 %), the performance of A1 over-expressing mice was always similar to control animals even during the most difficult task (i.e., 56/44 %). From these experiments, we conclude that A1 over-expressing mice had normal odour detection and discrimination abilities.

Short-term olfactory memory was evaluated by exposing mice only once to mint odorant (without previous habituation), followed by a second exposure to the same odorant after a 30-min interval (Fig. 2c). Wild-type mice spent less time investigating the odorant during the second exposure period (paired t test; $t_{(16)} = 2.907$, $p = 0.010$), indicating that they remembered the odorant and exhibited habituation. In contrast, transgenic mice spent more time exploring the odorant in the second exposure (paired t test;

$t_{(17)} = -4.469$, $p < 0.001$). Moreover, in this second exposure, A1 over-expressing mice also spent more time than wild-type mice ($t_{(33)} = -3.818$, $p < 0.001$). Similar results were obtained when another cohort of animals was tested and the rest period was 15 min (data not shown). These results show that A1 over-expression did not change olfactory perception but altered short-term olfactory memory.

Anosmin-1 over-expression increases OB interneuron density

The altered olfactory behaviour prompted us to investigate the effects of A1 over-expression on anatomical features of the different components of the olfactory system. First, we studied the olfactory epithelium and found no gross anatomical changes in transgenic mice compared with wild-type (data not shown). We quantified the OB volume using Cavalieri's method and found no difference in the volume of the entire structure or the different layers (Fig. 3a, b). We also analysed the rostro-caudal distribution of glomeruli per section in the OB, and found no significant difference between A1 over-expressing and wild-type animals (Fig. 3c). We next quantified the neuronal density of distinct populations (NeuN⁺, CR⁺, CB⁺, TH⁺ and PV⁺ cells) within the OB. The stereological analysis revealed a significant increase in the density of four GABAergic interneuron populations in A1 over-expressing mice compared to wild-type animals (Table 1). Thus, we found more mature NeuN⁺ interneurons in the granule cell layer of A1 over-expressing mice ($t_{(10)} = 2.932$, $p = 0.039$). Furthermore, there were more PV⁺ interneurons in the external plexiform layer ($t_{(4)} = 21.193$, $p < 0.001$) and CB⁺ neurons ($t_{(14)} = 2.369$, $p = 0.032$) and TH⁺ ($t_{(4)} = 3.420$, $p = 0.027$) in the glomerular cell layer (Table 1; Fig. 3d–e).

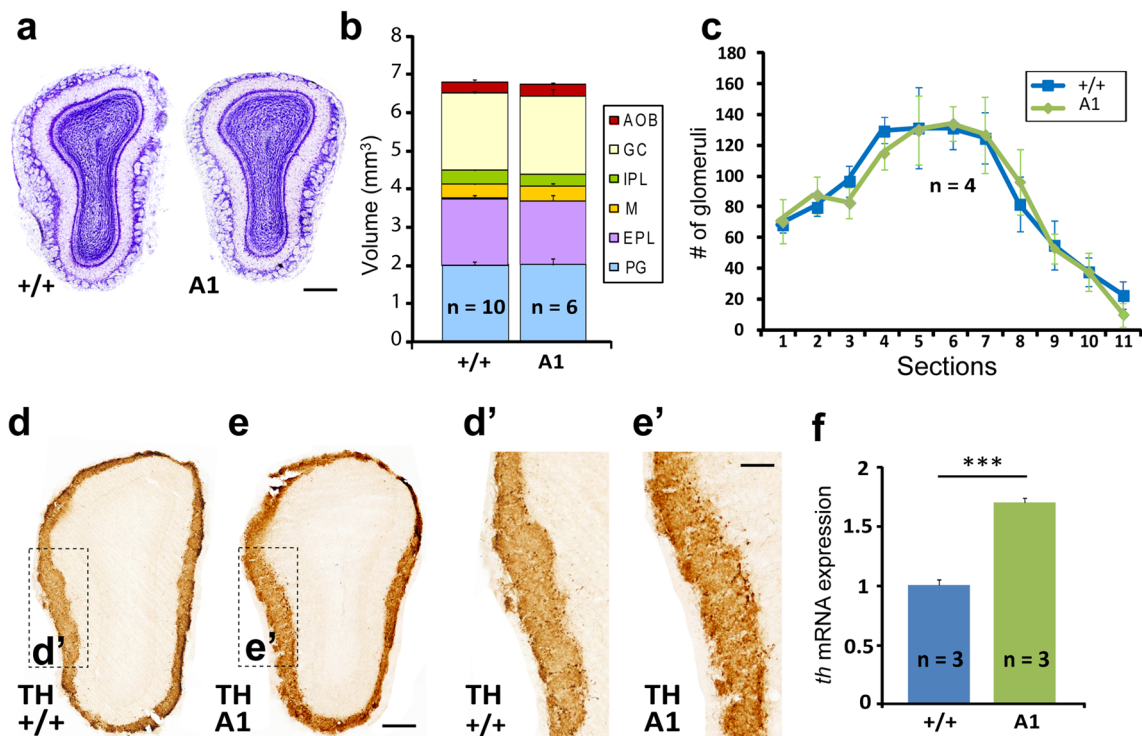


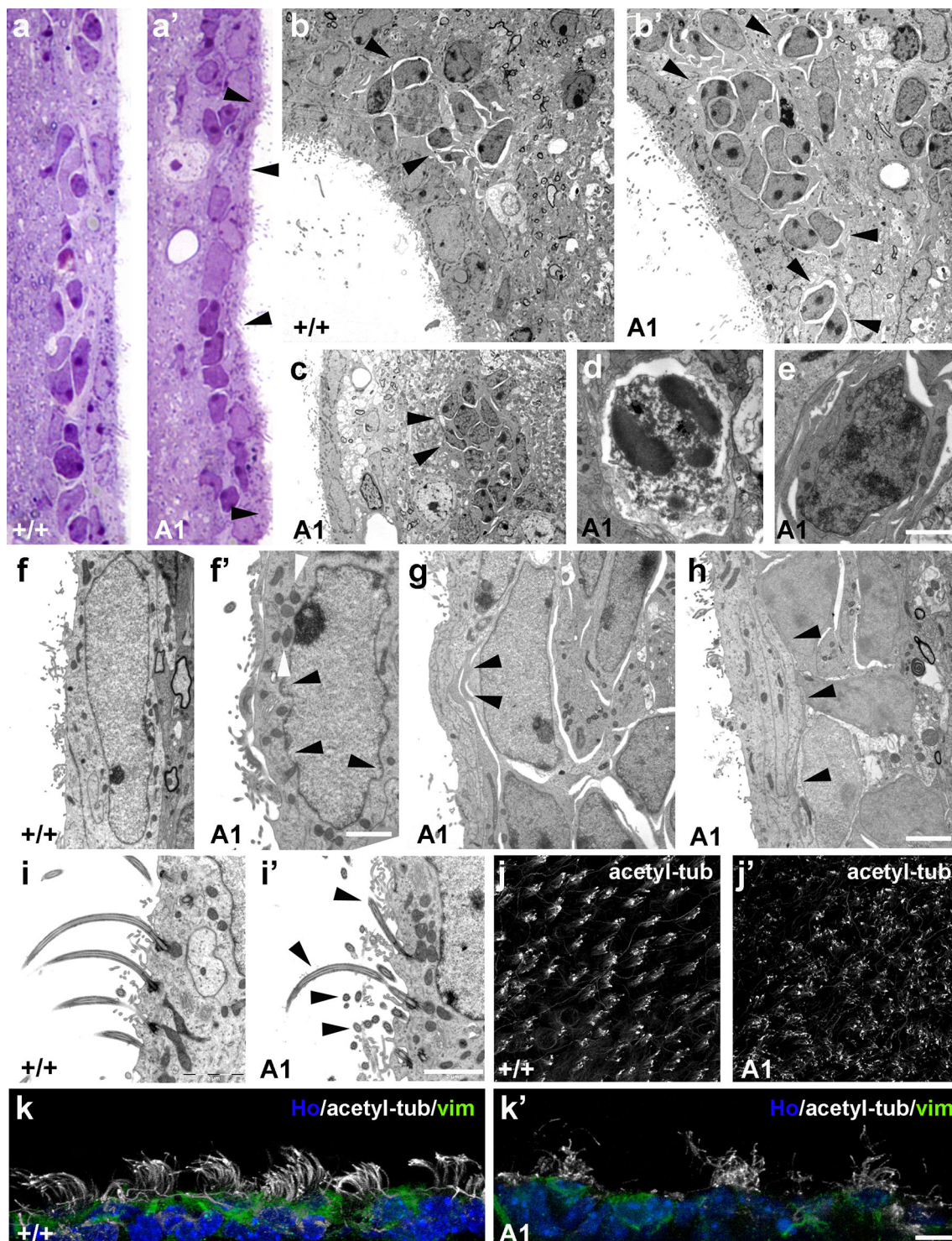
Fig. 3 No gross morphological differences in the OB of A1 over-expressing mice. **a** Nissl staining on coronal sections from mouse OBs revealed no gross morphological differences between wild-type and A1 over-expressing mice. **b** The stereological estimation of the OB volume and its layers by *Cavalieri's* method showed no changes in A1 over-expressing animals (control $n = 10$; A1 $n = 6$; Student's t test) compared with wild-type mice. **c** The rostro-caudal distribution of OB glomeruli was calculated and showed no differences between both genotypes ($n = 4$ for each group; two-way ANOVA). **d**, **e** Illustrative example of coronal sections from mouse OBs showing

increased expression of TH⁺ neurons in the OB glomerular cell layer in A1 over-expressing mice. **f** *Th* mRNA expression levels quantified by RT-PCR showed a significant increase in the OB of A1 over-expressing mice ($n = 3$ for each group; Student's t test; $t_{(4)} = -8.493$, $p < 0.001$). Data for quantified OB interneuron densities are presented in Table 1. *AOB* accessory olfactory bulb, *GC* granule cell layer, *IPL* internal plexiform layer, *M* mitral cell layer, *EPL* external plexiform layer, *GL* glomerular cell layer. Scale bar **a** 750 μm , **d**, **e** 500 μm , **e**, **g** 100 μm . Data are presented as mean \pm SEM

Table 1 Quantification of OB interneurons

$10^4 \text{ cells} \times \text{mm}^{-3}$	NeuN ⁺ ($n = 6$ mice/group)		Calretinin ⁺ ($n = 6$ mice/group)			
OB layers	+/+	A1	+/+	A1		
GL	24.4 \pm 4.1	21.2 \pm 2.5	12.4 \pm 1.6	10.5 \pm 1.2		
EPL	7.7 \pm 0.8	6.7 \pm 0.9	3.5 \pm 0.3	4.3 \pm 0.4		
GC	40.3 \pm 5.2	55 \pm 5.5 ($p = 0.039$)	9.5 \pm 0.7	10.5 \pm 1		
$10^4 \text{ cells} \times \text{mm}^{-3}$	Parvalbumin ⁺ ($n = 3$ mice/group)		Tyrosine hydroxylase ⁺ ($n = 3$ mice/group)		Calbindin ⁺ ($n = 8$ mice/group)	
OB layers	+/+	A1	+/+	A1	+/+	A1
GL	–	–	13.6 \pm 2.1	25.6 \pm 2.8 ($p = 0.027$)	8.8 \pm 1.3	15.4 \pm 2.5 ($p = 0.032$)
EPL	1.3 \pm 0.1	8.5 \pm 0.3 ($p < 0.001$)	–	–	2.2 \pm 0.1	3.2 \pm 0.4

The stereological analysis using the optical disector method revealed increased numbers of mature interneurons NeuN⁺ in the granule cell layer in A1 over-expressing mice ($t_{(10)} = 2.932$, $p = 0.039$). Similarly, in A1 mice more inhibitory interneurons PV⁺ were found in the external plexiform layer ($t_{(4)} = 21.193$, $p < 0.001$) and in the periglomerular cell layer, where CB⁺ ($t_{(14)} = 2.369$, $p = 0.032$) and TH⁺ ($t_{(4)} = 3.420$, $p = 0.027$) neurons. Mean \pm SEM is represented. Student's t test (as compared with wild-type mice). Illustrative images are shown in Fig. 3d, e



Moreover, qRT-PCR confirmed a higher expression level of *th* mRNA in the OB of A1 over-expressing mice (Student's *t* test; $t_{(4)} = -8.493$, $p < 0.001$; Fig. 3f). In contrast, the number of CR⁺ neurons did not differ between wild-type and transgenic mice (Table 1).

Anosmin-1 over-expression does not produce changes in OB mitral cells

Since A1 has been shown to be expressed in OB mitral cells (Clemente et al. 2008), we quantified the number of

Fig. 4 Morphological characterisation of the SVZ. **a** Pre-embedding toluidine blue immunostaining on semithin sections of coronal sections evidenced an irregular surface due to numerous protuberances in the SVZ of A1 over-expressing mice (see *arrowheads*). **b** Electron microscopy analysis showed an increased number of migratory and transit-amplifying cells (see *arrowheads*). **c** In A1 over-expressing mice, groups of neuroblasts (see *arrowheads*) were occasionally found at longer distances from the ventricle. High magnification example of mitotic (**d**) and pycnotic cells (**e**) that was observed with more frequency in A1 over-expressing mice. **f** High magnification images of the nuclear membrane of ependymal cells presented an irregular surface (*black arrowheads*) and a higher number of larger mitochondria (*white arrowheads*). **g** Clusters of neuroblasts in direct contact with ependymal cells produce narrowing of the ependymal layer and protuberances in transgenic animals (see *arrowheads*). **h** In A1 over-expressing mice, ependymal cells showed larger interdigitation processes (see *arrowheads*). **i** High magnification electron microscopy images illustrating altered orientation of ependymal cilia in A1 over-expressing mice (*black arrowheads* indicate disoriented cilia in **i'**). **j** Confocal images of whole mount preparations of the ventricular surface stained for acetylated tubulin. **k** Confocal images of coronal sections co-stained for acetylated tubulin and vimentin in control and A1 over-expressing mice. *Scale bar a* 10 μm , *b* 8 μm , *c* 7 μm , *d*, *e* 1 μm , *f* 2 μm , *g*, *h* 1 μm , *i* 2 μm , *j* 25 μm , *k* 10 μm

projection neurons (mitral cells) and found no difference (+/+ : 17.86 ± 1.39 ; A1: 18.58 ± 0.88 ; $t_{(4)} = -0.436$, $p = 0.685$). Additionally, A1 was previously shown to control axonal outgrowth of OB projection neurons, thereby playing an important role in axon guidance and collateral branching during development (Soussi-Yanicostas et al. 2002). Hence, we performed tracer injections in the OB to investigate alterations in the LOT (lateral olfactory tract, i.e., pathway containing mitral cell projections). There was no difference in collateral branches all along the LOT in A1 over-expressing compared with control mice (Suppl. Figure 1).

Anosmin-1 over-expression causes morphological alterations in the SVZ

Given the increased number of OB interneurons in A1 over-expressing mice, we studied the site of origin of these cells, namely the SVZ (Luskin 1993; Lois and Álvarez-Buylla 1994; Lois et al. 1996). We performed pre-embedding immunostaining in combination with electron microscopy to examine the cellular composition of the neurogenic niche (Fig. 4a). The SVZ lateral walls of A1 over-expressing mice exhibited an irregular surface and presented protuberances, corresponding with large groups of cells located underneath (Fig. 4a'). These clusters comprised highly packed transit-amplifying precursor and migratory cells (Fig. 4b). The number of intercellular spaces appeared increased, suggesting either enhanced proliferative or migratory activity (Fig. 4b'). We also found groups of isolated young neurons at longer distances from

the lumen of the ventricle (Fig. 4c), where we observed with higher frequency pycnotic and mitotic cells in transgenic animals (Fig. 4d, e).

Moreover, the analysis of the ultrastructure of ependymal cells in A1 over-expressing mice evidenced deeper interdigitations of the cell membrane with long lateral extensions as well as an irregular nuclear membrane and larger mitochondria size (Fig. 4f, f'). Occasionally, migratory cells were found to be in direct contact with ependymal cells, rendering the ependymal cell layer thinner as a consequence of the expansion of neuroblast and transit-amplifying precursor cell populations underneath (Fig. 4g, h). Interestingly, this abnormal morphology of the ependymal cells was also reflected in disoriented cilia (Fig. 4i, i'). To obtain an overall *en face* view of the ventricular surface, we performed SVZ wholemount dissections, as previously described (Mirzadeh et al. 2010a). In wild-type mice, acetylated tubulin staining revealed the usual *pinwheel* disposition of ependymal cells (Mirzadeh et al. 2008, 2010b). In A1 over-expressing mice, acetylated tubulin staining showed irregular and disorganised ependymal cilia (Fig. 4j, k').

FGFR1 expression in the SVZ

To better understand the effects of A1 over-expression in the SVZ, we analysed in detail the expression pattern of FGFR1. It has been reported that FGFR1 is expressed by radial glia in the developing cerebral cortex, and FGFR1-mediated signalling is highly conserved across species and supports many physiological functions, including the maintenance of the stem cell niche (Vacarino et al. 1999). In both wild-type and A1 over-expressing mice, we found that the vast majority of ependymal cells (nestin and/or vimentin⁺ cells) and many astrocytic GFAP⁺ cells within the SVZ express FGFR1 (Fig. 5a–d). Intriguingly, we also observed FGFR1 co-expression with the γ -tubulin-labelled basal body of the primary cilium (Fig. 5e–l), as recently described for IGFR1, which regulates ciliary resorption (Yeh et al. 2013). This would suggest a similar role for FGFR1 in primary cilium function when sensing not only FGFs but also secreted A1 in the cerebrospinal fluid (CSF). Besides, we also found FGFR1 expression in transit-amplifying precursor cells (Mash1⁺; Fig. 5m–p) as well as in neuroblasts (DCX⁺) both in the SVZ and inside the RMS (Fig. 5q–x).

Anosmin-1 over-expression stimulates neurogenesis in the SVZ by increasing the number of symmetric divisions

Quantification of proliferating cells in the SVZ in P80 animals evidenced a two-fold increase in the global number

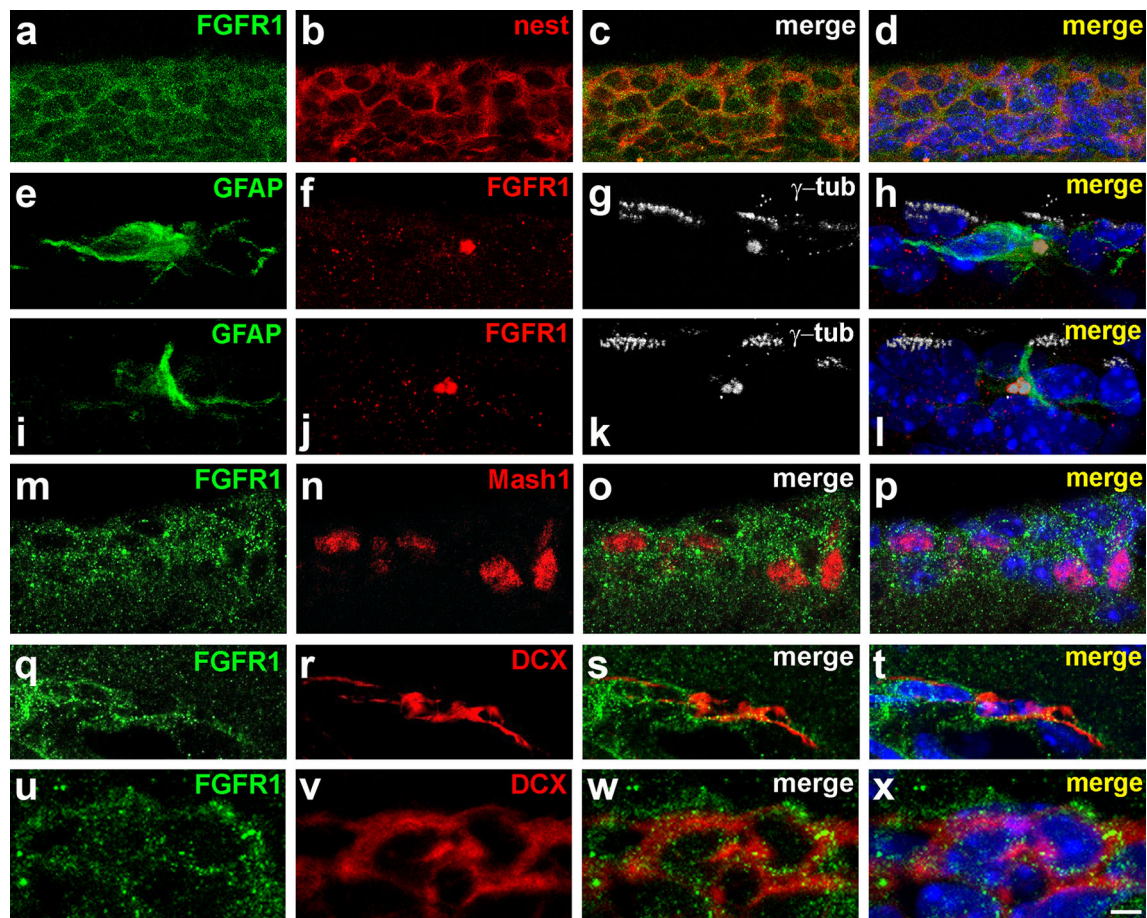


Fig. 5 Detailed expression pattern of FGFR1 in the SVZ. **a–d** Representative confocal images of coronal sections co-stained for FGFR1 and nestin in wild-type mice. **e–l** Two examples of high magnification confocal images showing the co-expression of FGFR1 and γ -tubulin at the basal body of primary cilia. **m–p** Transit-

amplifying cells also express FGFR1 within the SVZ. **q–t** Neuroblasts in the SVZ also present FGFR1. **u–x** Chains of neuroblasts in the RMS also express FGFR1. *Scale bar a–d* 10 μ m, *e–l* 2 μ m, *m–p* 8 μ m, *q–t* 5 μ m, *u–x* 2 μ m

of PH3⁺ (i.e., an M phase cell cycle marker) cells in A1 over-expressing mice ($t_{(6)} = 3.333$, $p = 0.029$; Fig. 6a–c). We next focused on migratory cells, which still retain a limited proliferative activity, and revealed by co-staining of PH3 with DCX antibody. Indeed, we found an enhanced rate of neuroblast proliferation in transgenic animals ($t_{(6)} = 3.432$, $p = 0.026$; Fig. 6d). Rarely, the increased proliferation resulted in hyperplasias that eventually broke the wall of ependymal cells and invaded the lumen of the ventricle (Fig. 6b1). At P60, we injected BrdU, and after 20 days, we quantified the presence of proliferating cells within the OB. We detected a significant increase in the number of cells that incorporated BrdU in A1 mice ($t_{(6)} = 6.761$, $p < 0.001$; Fig. 6e–g). When we quantified the relative density of apoptotic cells in the OB by labelling cells for cleaved caspase-3, we observed no difference between wild-type and transgenic mice (Suppl. Figure 2), indicating that the over-expression of A1 did not affect cell death. To further elucidate the cellular mechanism of

action of A1, we examined the behaviour of SVZ progenitor cells in cell culture with VTL imaging—in the absence of exogenous growth factors, such as FGF2 or EGF—and the total number of clones undergoing neurogenic divisions was estimated (Fig. 7a; Suppl. Figure 3). Surprisingly, we found a reduction in the relative number of neurogenic clones undergoing only one round of division (Fig. 7b). However, we observed a striking increased number of neurogenic clones that went through more than two rounds of symmetric divisions in A1 over-expressing mice in comparison with wild-type mice (Fig. 7b). This feature, characteristic of active transit-amplifying precursor cells, would explain the higher proliferative activity observed in A1 over-expressing mice. To provide functional evidence for the mechanism of action responsible for this increased proliferative activity, we assessed BrdU incorporation in dissociated cell cultures assays by blocking FGFR activity with the inhibitor SU5402 (10 μ M) in the absence of exogenous growth factors. In SVZ-derived

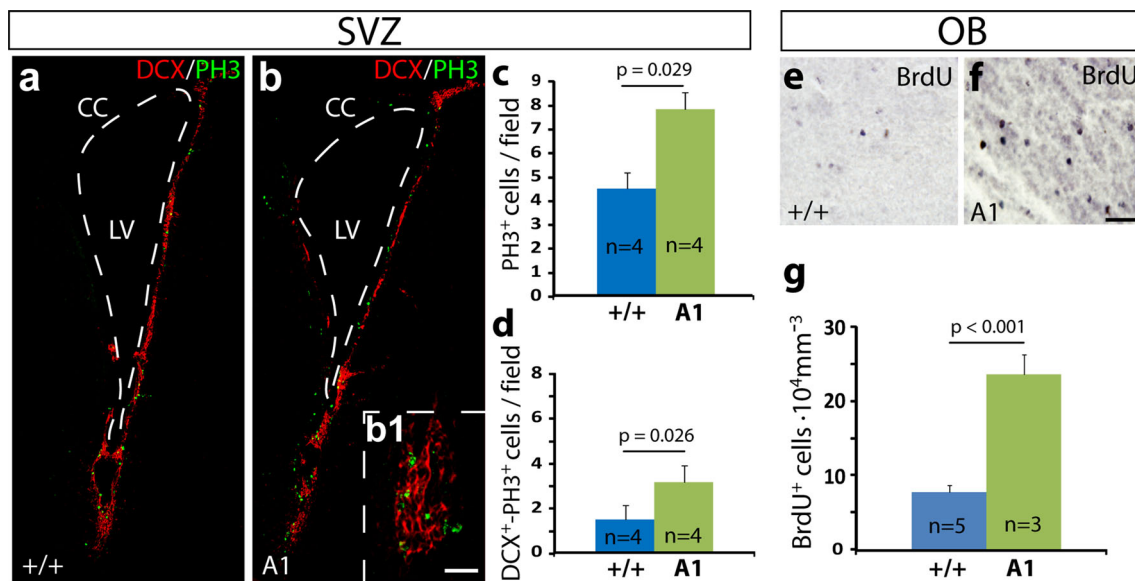


Fig. 6 Anosmin-1 over-expression enhances proliferation in the SVZ. **a, b** Confocal images of coronal sections co-stained for PH3 and DCX. **b1** Onset of an illustrative hyperplasia co-stained for PH3 and DCX found in A1 over-expressing mice. **c** Quantification of proliferating cells in the SVZ showing more PH3⁺ cells in A1 over-expressing mice in (Student's *t* test; $t_{(6)} = 3.333$, $p = 0.029$).

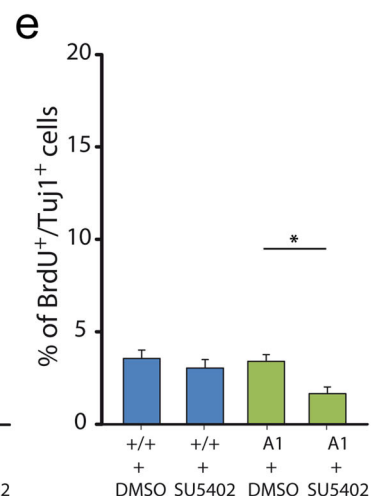
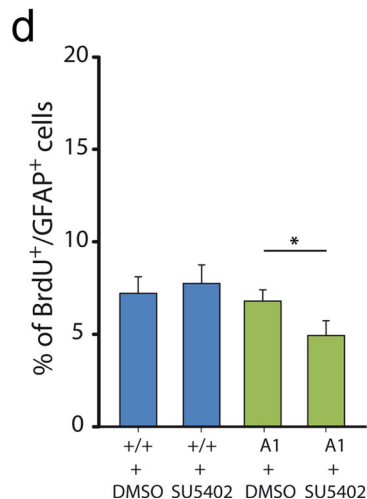
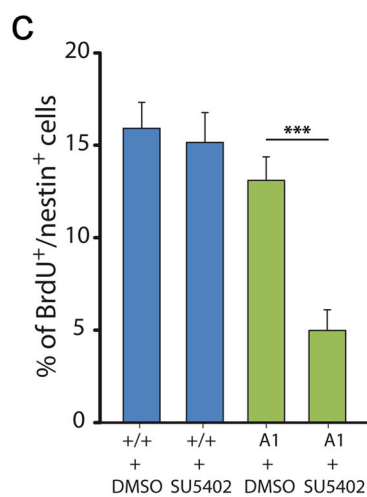
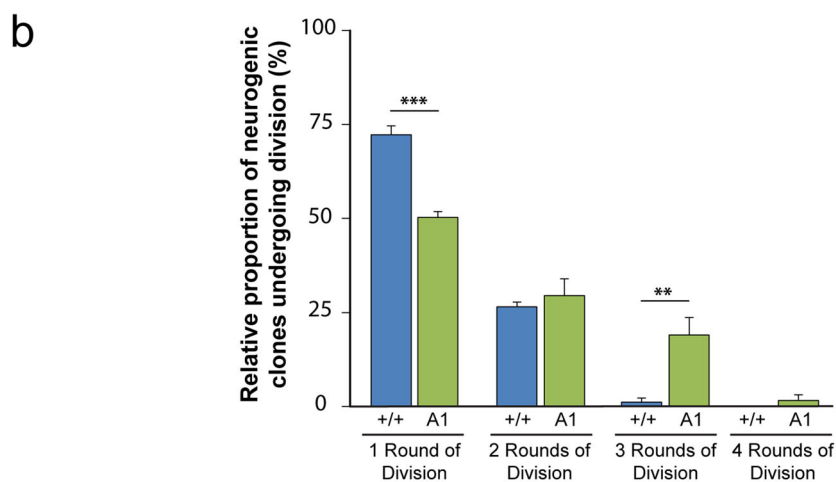
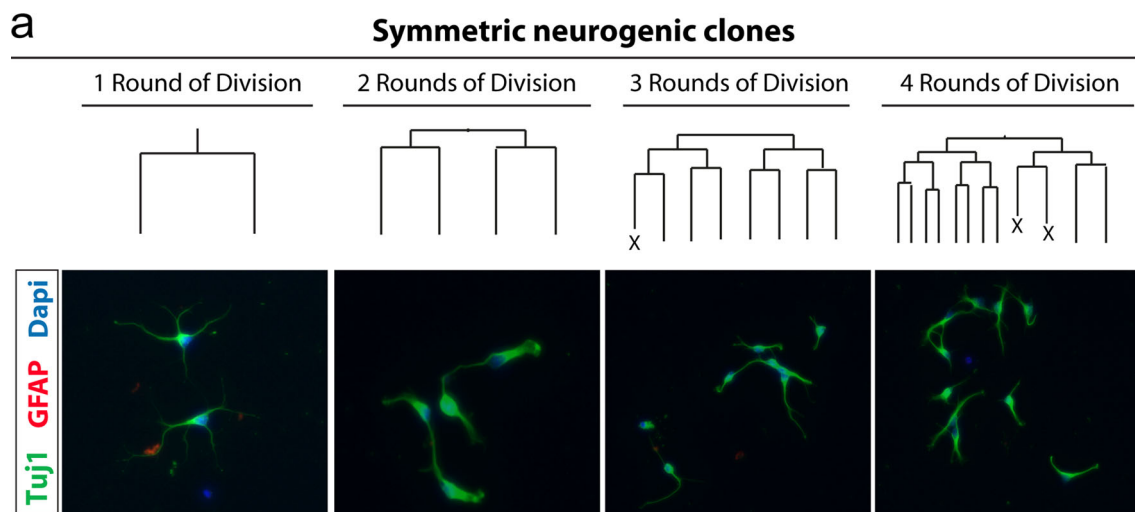
d Quantification of proliferating neuroblasts co-stained with PH3 and DCX antibodies (Student's *t* test; $t_{(6)} = 3.432$, $p = 0.026$). **e, f** Bright field microscope images BrdU⁺ cells within the OB. **g** Quantification of BrdU incorporation in the OB (Student's *t* test; $t_{(6)} = 6.761$, $p < 0.001$). Scale bar **a, b** 100 μm , **b1** 20 μm , **e, f** 30 μm . Data are presented as mean \pm SEM

cells from +/+ mice, we found no differences between untreated and treated conditions regarding proliferation for the three cell populations analysed: neuronal precursor cells (nestin⁺), astrocytes more differentiated (GFAP⁺) and finally neuroblasts (Tuj1⁺; Fig. 7c–e). However, in the case of cells derived from A1 over-expressing mice, in the presence of SU5402, we found a consistent decrease in the number of proliferating cells in all three populations (Fig. 7c–e). This would suggest that FGFR activity was endogenously enhanced in A1 over-expressing mice since no external growth factor was added to the cell medium and the concentration of FGF2 endogenously produced by cultured cells should be almost insignificant. Together these results suggest that the higher neurogenic activity observed in A1 mice was caused by an increased activation of FGFR1 neural progenitor cells, mainly in transit-amplifying precursor cells in the SVZ.

Anosmin-1 over-expression increases SVZ neuroblast migration in vitro

We previously described a FGFR1-mediated chemoattractant effect of exogenous A1 on rat SVZ neuroblasts during embryonic and postnatal development (García-González et al. 2010; Murcia-Belmonte et al. 2010; Esteban et al. 2013). To dissect whether the increased density of interneurons and BrdU⁺-cells within the OB was only the consequence of enhanced proliferation in the SVZ, or

might also reflect modification of neuroblast migratory behaviour, we performed functional in vitro experiments. Using chemotaxis chambers, we confirmed our own previous observations on wild-type and transgenic mice, finding that A1 was able to exert the same chemotactic effect on SVZ neuronal precursors (Suppl. Figure 4). To determine the influence of A1 over-expression on neuroblast migration, we cultivated SVZ explants in collagen matrix without any supplementary cue to evaluate neuroblast intrinsic motility. The neuronal identity of migrating cells was ascertained based on Tuj1⁺/DCX⁺/Olig2⁻/GFAP⁻ immunoreactivity, and the occurrence of proliferation in migrating cells was discarded as the cause of higher migration rates by co-labelling for Tuj1 and PH3 (Suppl. Figure 5). Explant cell migration was analysed by calculating the area occupied by migrating neuroblasts and the migration index (M.I.: final explant area divided by the initial surface). Explants from A1 mice evidenced a higher MI ($t_{(121)} = 3.359$, $p = 0.001$; Fig. 8a–c) suggesting an increased migratory ability. To further investigate the dynamic temporal aspects of the differences in migratory properties, we analysed the behaviour of migrating SVZ neuroblasts using VTL imaging. Cell movements were saltatory, with displacements interrupted by stationary periods, and followed a radial dispersion pattern, mostly individually but also in chains, when migrating out from explants (Fig. 8d, e). Interestingly, in explants from A1 over-expressing mice individual cell tracking revealed a



lower amount of stationary periods ($t_{(663)} = 3.256$, $p = 0.001$; Fig. 8f) and a significant increase in the average velocity ($t_{(663)} = 13.754$, $p < 0.001$; Fig. 8g), as well as in the total distance covered by A1 neuroblasts (two-way ANOVA; Genotype \times Time; $F_{(1,143)} = 212.025$,

$p_{\text{genotype}} < 0.001$; Bonferroni post hoc t test +/+ vs. A1; $t = 14.487$, $p < 0.001$; Fig. 8h, i). To further elucidate the molecular mechanism, in chemotaxis assays we blocked FGFR activity with the inhibitor SU5402 (10 μM) and found a reduced number of migrating neuroblasts (Tuji1⁺;

Fig. 7 Anosmin-1 over-expression increases symmetric divisions. Increased rounds of amplifying divisions within the symmetric neurogenic clones in SVZ cultures of A1-overexpressing mice. SVZ cultures isolated from wild-type or A1 over-expressing mice were continuously imaged by time-lapse video microscopy for 6 days. **a** Total amount of clones undergoing neurogenic divisions were tracked per cover slip. Examples of symmetric neurogenic clones undergoing 1, 2, 3 or 4 rounds of amplifying divisions, respectively. Post-imaging immunocytochemistry confirmed the neuronal nature of the progeny (β III-tubulin positive cells). **b** Histogram depicting the relative proportion of neurogenic clones undergoing division in both wild-type and A1 conditions. Note the increase in the rounds of neurogenic amplifying divisions in A1-overexpressing mice compared to controls. Total amount of clones analysed: 180. **c–e** Histograms illustrating the percentage of nestin, GFAP and Tuj1⁺ cells that incorporate BrdU (50 μ M) in dissociated cell cultures experiments per field. At least 200 different fields were analysed in total from 3 independent experiments for each cell population (ANOVA, Tukey post hoc test; *** $p < 0.001$, ** $p < 0.01$, * $p < 0.05$)

Fig. 8j–k). Altogether, these data indicate that A1 over-expression increases SVZ neuroblast intrinsic motility via FGFR1 activity, and confirm the biological effect of A1 as a chemoattractant cue on SVZ neuroblasts in mice, previously reported in rats.

Discussion

Anosmin-1 intervenes in a wide range of processes in the CNS

Although the biological effects of A1 have been investigated mainly during neural development, little is still known about its effects in the adult brain. The present work is the first to report that A1 strongly stimulates neurogenesis in the SVZ and also augments subsequent neuroblast motility in adult mice. Previous studies have shown that A1 is involved in diverse fundamental biological processes such as cell migration, axon guidance, dendritic branching, and tumour growth (Bülow et al. 2002; Soussi-Yanicostas et al. 2002; Cariboni et al. 2004; Andrenacci et al. 2006; García-González et al. 2010; Choy et al. 2013).

In the adult rodent brain, the basal lamina of the ventricle walls represents an extensive source of signals controlling progenitor cell behaviour, pointing to the ECM as an emerging regulator of the effects of contact-mediated and secreted signals (Mercier et al. 2002; Shen et al. 2008; Tavazoie et al. 2008; Snayyan et al. 2009; Kokovay et al. 2010). In addition, it has been reported that ECM microstructures in the wall of the lateral ventricles with high levels of heparan sulphate proteoglycan immunoreactivity, called fractones, can directly control FGF2 local availability (Kerever et al. 2007). Another recent study described how A1 promotes neural crest formation by controlling FGF8 activity (Endo et al. 2012). Together, these reports

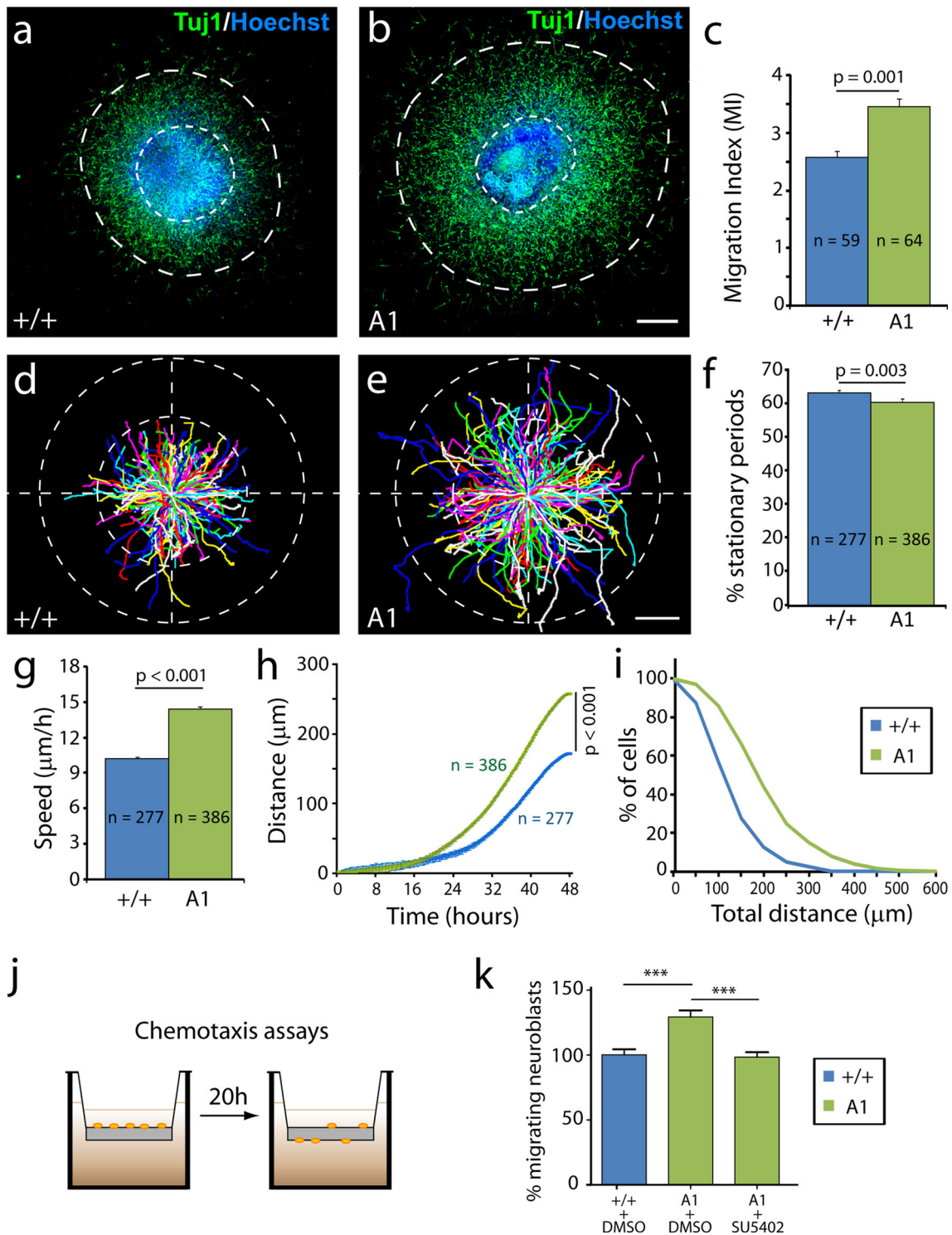
highlight the relevance of ECM molecules in general and of A1 in this particular case in regulating growth factor activity, whose relevance might have been underestimated so far.

FGFR1 is expressed in the SVZ and plays specific roles in each cell type

The presence of FGFR1 has been documented in almost all SVZ cell types in wild-type animals (Gritti et al. 1999; García-González et al. 2010), whereas A1 expression is only restricted to neuroblasts (García-González et al. 2010). During embryonic development, FGFR1 is highly expressed in radial glial cells (Zheng et al. 2004) and in adult animals is prominently associated with neural progenitor cells (Gálvez-Contreras et al. 2012), determining neuronal and oligodendroglial cell fate (Andrenacci et al. 2006; Anderson et al. 2007; Furusho et al. 2011; Gálvez-Contreras et al. 2012). Interestingly, mice lacking FGFR1 show a global decrease in radial glia and oligodendroglial progenitors (Ohkubo et al. 2004) and present a reduced OB due to telencephalic morphogenesis defects (Hébert et al. 2003), similarly to KS patients (Dodé and Hardelin 2009).

Within the SVZ, ependymal cells provide physical, trophic and metabolic support for progenitor cells, conforming a polarised cell layer with oriented bundles of motile cilia in contact with the ventricle lumen (Del Bigio 2010). Notably, radial glia and their progeny (ependymal and neural progenitor cells) strongly express FGFR1 (Zheng et al. 2004; García-González et al. 2010; Gálvez-Contreras et al. 2012) and FGFR1 signalling regulates cilia length and function in diverse epithelia during development (Neugebauer et al. 2009). Moreover, FGFR1 is expressed in the motile cilia and FGF signalling is associated with tumour progression and several ciliopathies (Trumpp et al. 1999; Evans et al. 2002; Macatee et al. 2003; Creuzet et al. 2004; Szabo-Rogers et al. 2008; Zaghoul and Brugmann 2011). Hence, FGFR1 expression in ependymal cells may actually be important for ependymal ciliary beating in the lateral ventricles. Therefore, this would explain the differences observed not only in the shape of the nuclear membrane but also in the larger size of mitochondria in A1 over-expressing mice, where alterations in ciliary beating movements may underlie an enhanced local metabolic activity.

It has been shown that the primary cilium acts as a mechano- and chemoreceptor sensing flux changes and chemicals in the CSF for a subpopulation of adult neural progenitor cells (Han et al. 2009; Lehtinen et al. 2011; Li et al. 2011a; Yeh et al. 2013). Several studies have identified circulating morphogens and growth factors in the CSF, such as Shh, PDGF-AA, IGF1, Wnt and FGF2, which have been found responsible for normal CNS patterning



(Raballo et al. 2000; Nusse 2003; Martin et al. 2006; Han et al. 2009; Lehtinen et al. 2011). The present work is the first to report co-expression of FGFR1 and γ -tubulin in primary cilium basal body in the SVZ, allowing us to speculate about the role of FGFR1 regulating primary cilium length and function and, therefore, directly controlling

proliferation in the neurogenic niche. Additionally, the increased number of symmetric neurogenic divisions in transit-amplifying precursor cells and the significant reduction of proliferation upon the blockade of FGFR activity in cells over-expressing A1, suggests that FGFR1 expression in the SVZ renders A1 a key element to regulate

Fig. 8 Anosmin-1 over-expression increases SVZ neuroblast motility. **a, b** SVZ explants embedded in collagen matrix from P0 mice were stained with Tuj-1 and DCX antibodies. Neuroblasts migrated following a radial dispersion pattern mostly individually but also forming chains. **c** Quantification of the migration, represented as Migration Index, considered as the final area occupied by migrating neuroblasts divided by the initial explant surface (Student's *t* test; $t_{(121)} = 3.359$, $p = 0.001$). **d, e** Representation of the trajectories covered by migrating neuroblasts in video time-lapse experiments. **f** Quantification of the percentage of stationary periods (Student's *t* test; $t_{(663)} = 3.256$, $p = 0.003$). **g** Speed migration was also higher in A1 over-expressing mice (Student's *t* test; $t_{(663)} = 13.754$, $p < 0.001$). **h** The same effect can be observed in the evolution of the migrated distance along time (two-way ANOVA; Genotype \times Time; $F_{(1,143)} = 212.025$, $p_{\text{genotype}} < 0.001$; Bonferroni post hoc *t* test Wt vs. A1; $t = 14.487$, $p < 0.001$) and in the **i** cumulative plot illustrating the percentage of neuroblasts that migrated a certain distance. **j** Scheme depicting the procedure used for chemotaxis assays in Boyden chambers with SVZ-derived dissociated cells. **k** SVZ A1-over-expressing neuroblasts (Tuj1⁺) placed in the upper compartment of Boyden chambers migrated more than neuroblasts from wild-type animals. The presence of the FGFR inhibitor SU5402 (10 μ M) reduced the migration of neuroblasts Tuj1⁺ derived from A1 over-expressing mice (ANOVA, Tukey post hoc test; *** $p < 0.001$). Data are presented as mean \pm SEM. Scale bar **a, b, d, e** 200 μ m

its activity, although we cannot exclude the possibility that other receptors might also be involved. In this sense, the existence of homophilic interactions between anosmin-1 also seems a plausible explanation since it has been shown to exert biological effects (Murcia-Belmonte et al. 2010). Thus, our data indicate that the overall increase in proliferation in A1 over-expressing mice was mainly due to the interaction of A1 with FGFR1 and highlight the relevance of the ECM composition in the neurogenic niche.

Anosmin-1 increases SVZ neuroblast motility

In rodents, neurogenesis persists in the healthy adult brain in the SVZ, where newborn cells generated in the SVZ migrate to the OB where they become mature interneurons (Lois and Álvarez-Buylla 1994; De Marchis et al. 2007; Nissant et al. 2009). Our previous work identified two more cues dynamically involved in this process: FGF2 and A1, which promote neuroblast migration during embryonic and postnatal development (García-González et al. 2010). Indeed, the complex combination of molecular cues driving neuroblast migration from embryonic development to adulthood, based on secreted chemoattractants and chemorepellents, is far from being completely understood (for reviews see: Ghashghaei et al. 2007; Pignatelli and Belluzzi 2010). In the present study, we show how A1 over-expression alone increases SVZ neuroblast motility via FGFR1 activity, without the presence of other exogenous cues, suggesting that A1 plays an important role in cell–cell and cell–substrate interactions.

Anosmin-1 over-expression determines a change of OB neuronal densities and causes alterations in olfactory memory

Once in the OB, neuroblasts differentiate in a wide range of interneurons, differing in localisation, morphology, neurochemistry and synaptic properties, and modulate olfactory epithelium inputs (Shipley and Adamek 1984; Kosaka and Kosaka 2005; Parrish-Aungst et al. 2007). Although it has been proposed that the functional diversity of newborn interneurons serves to given purposes, little is known about this specificity in detail. The overwhelming majority of granular, periglomerular and external plexiform interneurons are GABAergic. Precisely, periglomerular cells can be further subdivided into three non-overlapping populations: TH⁺, CB⁺ and CR⁺ interneurons (for a review: Ledó et al. 2008). This diversity in OB interneuron populations reflects a wide range of molecular heterogeneity associated to spatial subdomains in the SVZ, already existing in migrating neuroblasts that determines their final identity before reaching the OB (Ledó et al. 2008). During embryonic development, the origin of OB interneurons has been traditionally linked with the lateral ganglionic eminence (LGE), a subpallial region that contributes to form the SVZ of the lateral ventricles in the telencephalon (Wichterle et al. 2001). Although there is a significant proportion of progenitor cells derived from pallial regions that populate the OB, it has been shown that the majority of olfactory interneurons originate from progenitors expressing subpallial markers (Kohwi et al. 2007; Young et al. 2007). Interestingly, LGE-derived progenitors give rise to the majority of OB interneuron populations that we have found increased in A1-over-expressing mice: periglomerular (TH⁺ and CB⁺) and external plexiform interneurons (PV⁺) (Kosaka and Kosaka 2005; Kohwi et al. 2007; Young et al. 2007; Li et al. 2011b). By contrast, in the case of CR⁺ cells, whose origin emerges mainly from pallial and septal progenitors and not from the LGE (Kosaka and Kosaka 2005; Kohwi et al. 2007; Young et al. 2007; Li et al. 2011b), no difference was observed in any OB layer. Regarding the temporal generation of OB interneurons, it has been reported that the majority of TH⁺, CB⁺ and PV⁺ interneurons are already produced postnatally, with a lower turnover rate than CR⁺ cells in adult mice (Kohwi et al. 2007; Young et al. 2007; Batista-Brito et al. 2008). To note, four novel subtypes of interneuron generated in specific SVZ microdomains only postnatally have been recently identified (Merkle et al. 2014). To have a better understanding of the complex spatial and temporal behaviour of SVZ neural progenitor cells, further analysis is still necessary. Altogether, these lines of evidence indicate that the changes reported in the OB of adult mice over-

expressing anosmin-1 may arise from LGE-derived progenitor cells.

Thus, the overall increase in the number of GABAergic interneuron populations in A1 over-expressing mice together with the lack of obvious changes in OB excitatory cells and projections, strongly suggest alterations in the normal processing of olfactory information since these inhibitory interneuron populations act at different levels in the OB local circuitry. More specifically, the subpopulation of TH⁺ periglomerular cells plays a major role in the inhibition of sensory inputs from olfactory sensory neurons since they receive direct synaptic contacts from the olfactory epithelium and dynamically respond to significant changes in olfactory activity in rodents and primates (Stone et al. 1991; Kosaka and Kosaka 2005; Liberia et al. 2013). Consistent with this finding, the loss of functional sensory inputs in rodents results in a profound decrease in the expression of TH⁺ periglomerular cells (Briñón et al. 2001; Song and Leonard 2005). Conversely, the upregulation of TH has extensively been linked to severe olfactory problems in different neurodegenerative conditions, such as Parkinson's disease, Alzheimer's disease and fronto-temporal dementia, suggesting a finely tuned activity in TH⁺ cells (Hawkes 2003; Kovacs 2004; Mundiñano et al. 2011). This sensory loss is not a consequence of damages in the olfactory epithelium, but rather a result from distinct abnormalities in the OB, such as protein deposits or changes in interneuron densities (Hawkes 2003; Kovacs 2004; Mundiñano et al. 2011). A mechanism of action involving FGFR1 signalling in neuronal differentiation to a dopaminergic phenotype would be consistent with our data since a dominant negative FGFR1 expressed under the control of the TH promoter gives rise to a decreased number of TH⁺ cells (Klejbor et al. 2006). In this sense, more recent findings in a loss-of-function model in zebrafish have also shown that the lack of A1 leads to a specific reduction of the number of TH⁺ and GABAergic OB interneurons (Yanicostas et al. 2009). It has been proposed that TH⁺ periglomerular cells in the OB have a key impact on the processing of olfactory information by switching off the entrance of sensory information from the terminals of the olfactory nerve (Gutiérrez-Mecinas et al. 2005). Thus, the increased density of TH⁺ periglomerular cells in A1 over-expressing mice would explain the impaired olfactory behaviour.

Accumulating evidence indicates that changes in adult SVZ neurogenesis have diverse effects on olfactory processing. In agreement with our data, previous reports suggested that alterations in the number of OB interneurons and, therefore, in the excitatory-inhibitory balance, have little or no impact on odorant perception and discrimination although short-term olfactory memory results impaired (Breton-Provencher et al. 2009; Lazarini et al. 2009;

Lazarini and Lledó 2011). However, a recent study showed that connective tissue growth factor derived from excitatory tufted neurons regulates the survival of OB periglomerular interneurons and modulates olfactory perception and discrimination, but not long-term olfactory memory (Khodosevich et al. 2013). Indeed, differences between each experimental approach and behavioural paradigm constrain our analysis and do not allow us to be more conclusive since the precise functional relevance of adult neurogenesis still remains an unresolved question in the field. Indeed, we are aware that the “olfactory memory” is a complex process not exclusively “olfactory” and other brain areas receiving projections from the piriform cortex—including neurogenic structures such as the hippocampus—may also be involved (for a review: de Castro 2009). However, to our understanding, their study would escape the scope of the present work. Given that the OB is the first telencephalic structure involved in the integration and processing of olfactory information, small alterations in specific OB interneuron populations may have a critical repercussion and would be sufficient to cause behavioural changes, as well as pathologies related to this sensory system.

Finally, the ECM is a key component of the cellular microenvironment since all cells make contact with different ECM elements. Although the functions of ECM molecules in neurogenic niches and in cell migration and differentiation have been largely investigated (for specific reviews: Ghashghaei et al. 2007; Hynes 2009), we still have a limited understanding of these processes. The present work reports for the first time a mouse model over-expressing the ECM glycoprotein A1, highlights the relevance of A1 functions and shows how A1 regulates adult neurogenesis in the olfactory system. However, the existence of a complex and coordinated crosstalk between ECM molecules with heparan sulphate proteoglycans, growth factors, integrins, cytokines and tyrosine kinase receptors (Kazanis and French-Constant 2011; Brizzi et al. 2012) hampers the current understanding of ECM roles and, therefore, further research in this direction is required.

Acknowledgments We thank Dr. José Ángel Rodríguez Alfaro and Dr. Javier Mazarío for their assistance with the confocal microscopy and Isabel Machín, Jacinto Sarmentero and Iris Sánchez for their technical support. We are also thankful to Prof. Hannah Monyer for her comments on the manuscript. This research was supported by grants from the Spanish *Ministerio de Economía, Innovación y Competitividad MINECO* (SAF2009-07842, ADE10-0010, RD07-0060-2007, RD12-0032-12 and SAF2012-40023 to FdC; and BFU2010-18284 to JMG-V), *FISCAM (Gobierno de Castilla-La Mancha, Spain—Grant Number PI2007-66)*, the Junta de Castilla y León (Spain, to EW), and from the *Fundación Eugenio Rodríguez Pascual* (Spain) to FdC. DGG and VMB were PhD students hired by *Gobierno de Castilla-La Mancha* (MOV2010-JI/11 and MOV2007-JI/19, respectively). FdCS is a CSIC staff scientist in special permission hired by *SESCAM (Gobierno de Castilla-La Mancha, Spain)*.

PFE was a researcher hired by *SESCAM (Gobierno de Castilla-La Mancha)* and ADE10-0010.

References

- Aguirre A, Gallo V (2004) Postnatal neurogenesis and gliogenesis in the olfactory bulb from NG2-expressing progenitors of the subventricular zone. *J Neurosci* 24(46):10530–10541. doi:[10.1523/JNEUROSCI.3572-04.2004](https://doi.org/10.1523/JNEUROSCI.3572-04.2004)
- Álvarez-Buylla A, Lim DA (2004) For the long run: maintaining germinal niches in the adult brain. *Neuron* 41(5):683–686 pii: S0896627304001114
- Anderson L, Burnstein RM, He X, Luce R, Furlong R, Foltynic T, Sykacek P, Menon DK, Caldwell MA (2007) Gene expression changes in long term expanded human neural progenitor cells passed by chopping lead to loss of neurogenic potential in vivo. *Exp Neurol* 204(2):512–524. doi:[10.1016/j.expneurol.2006.12.025](https://doi.org/10.1016/j.expneurol.2006.12.025)
- Andrenacci D, Grimaldi MR, Panetta V, Riano E, Rugarli EI, Graziani F (2006) Functional dissection of the Drosophila Kallmann's syndrome protein DmKal-1. *BMC Genet* 7:47. doi:[10.1186/1471-2156-7-47](https://doi.org/10.1186/1471-2156-7-47)
- Batista-Brito R, Close J, Machold R, Fishell G (2008) The distinct temporal origins of olfactory bulb interneuron subtypes. *J Neurosci* 28(15):3966–3975. doi:[10.1523/JNEUROSCI.5625-07.2008](https://doi.org/10.1523/JNEUROSCI.5625-07.2008)
- Breton-Provencher V, Lemasson M, Peralta MR 3rd, Saghatelian A (2009) Interneurons produced in adulthood are required for the normal functioning of the olfactory bulb network and for the execution of selected olfactory behaviors. *J Neurosci* 29(48):15245–15257. doi:[10.1523/JNEUROSCI.3606-09.2009](https://doi.org/10.1523/JNEUROSCI.3606-09.2009)
- Bribián A, Barallobre MJ, Soussi-Yanicostas N, de Castro F (2006) Anosmin-1 modulates the FGF-2-dependent migration of oligodendrocyte precursors in the developing optic nerve. *Mol Cell Neurosci* 33(1):2–14. doi:[10.1016/j.mcn.2006.05.009](https://doi.org/10.1016/j.mcn.2006.05.009)
- Bribián A, Esteban PF, Clemente D, Soussi-Yanicostas N, Thomas JL, Zalc B, de Castro F (2008) A novel role for anosmin-1 in the adhesion and migration of oligodendrocyte precursors. *Dev Neurobiol* 68(13):1503–1516. doi:[10.1002/dneu.20678](https://doi.org/10.1002/dneu.20678)
- Briñón JG, Crespo C, Weruaga E, Martínez-Guijarro FJ, Aijón J, Alonso JR (2001) Bilateral olfactory deprivation reveals a selective noradrenergic regulatory input to the olfactory bulb. *Neuroscience* 102(1):1–10 pii: S0306-4522(00)00443-7
- Brizzi MF, Tarone G, Defilippi P (2012) Extracellular matrix, integrins, and growth factors as tailors of the stem cell niche. *Curr Opin Cell Biol* 24(5):645–651. doi:[10.1016/j.ceb.2012.07.001](https://doi.org/10.1016/j.ceb.2012.07.001)
- Bülow HE, Berry KL, Topper LH, Peles E, Hobert O (2002) Heparan sulfate proteoglycan-dependent induction of axon branching and axon misrouting by the Kallmann syndrome gene kal-1. *Proc Natl Acad Sci USA* 99(9):6346–6351. doi:[10.1073/pnas.092128099](https://doi.org/10.1073/pnas.092128099)
- Cariboni A, Pimpinelli F, Colamarino S, Zaninetti R, Piccolella M, Rumio C, Piva F, Rugarli EI, Maggi R (2004) The product of X-linked Kallmann's syndrome gene (KAL1) affects the migratory activity of gonadotropin-releasing hormone (GnRH)-producing neurons. *Hum Mol Genet* 13(22):2781–2791. doi:[10.1093/hmg/ddh309](https://doi.org/10.1093/hmg/ddh309)
- Cavalieri B (1966) Geometria degli indivisibile. Unione Tipografico-Editrice Torino, Turin
- Choy CT, Kim H, Lee JY, Williams DM, Palethorpe D, Fellows G, Wright AJ, Laing K, Bridges LR, Howe FA, Kim SH (2013) Anosmin-1 contributes to brain tumor malignancy through integrin signal pathways. *Endocr Relat Cancer*. doi:[10.1530/ERC-13-0181](https://doi.org/10.1530/ERC-13-0181)
- Clemente D, Esteban PF, Del Valle I, Bribián A, Soussi-Yanicostas N, Silva A, de Castro F (2008) Expression pattern of Anosmin-1 during pre- and postnatal rat brain development. *Dev Dyn* 237(9):2518–2528. doi:[10.1002/dvdy.21659](https://doi.org/10.1002/dvdy.21659)
- Clemente D, Ortega MC, Arenzana FJ, de Castro F (2011) FGF-2 and Anosmin-1 are selectively expressed in different types of multiple sclerosis lesions. *J Neurosci* 31(42):14899–14909. doi:[10.1523/JNEUROSCI.1158-11.2011](https://doi.org/10.1523/JNEUROSCI.1158-11.2011)
- Creuzet S, Schuler B, Couly G, Le Douarin NM (2004) Reciprocal relationships between Fgf8 and neural crest cells in facial and forebrain development. *Proc Natl Acad Sci USA* 101(14):4843–4847. doi:[10.1073/pnas.0400869101](https://doi.org/10.1073/pnas.0400869101)
- de Castro F (2009) Wiring olfaction: the cellular and molecular mechanisms that guide the development of synaptic connections from the nose to the cortex. *Front Neurosci* 3:52. doi:[10.3389/neuro.22.004.2009](https://doi.org/10.3389/neuro.22.004.2009)
- De Marchis S, Bovetti S, Carletti B, Hsieh YC, Garzotto D, Peretto P, Fasolo A, Puche AC, Rossi F (2007) Generation of distinct types of periglomerular olfactory bulb interneurons during development and in adult mice: implication for intrinsic properties of the subventricular zone progenitor population. *J Neurosci* 27(3):657–664. doi:[10.1523/JNEUROSCI.2870-06.2007](https://doi.org/10.1523/JNEUROSCI.2870-06.2007)
- de San Maestre, Juan A (1856) Teratología: falta total de los nervios olfatorios con anosmia en un individuo en quien existía una atrofia congénita de los testículos y el miembro viril. *El Siglo Médico* 3:211–221
- Del Bigio MR (2010) Ependymal cells: biology and pathology. *Acta Neuropathol* 119(1):55–73. doi:[10.1007/s00401-009-0624-y](https://doi.org/10.1007/s00401-009-0624-y)
- Díaz D, Lepousez G, Gheusi G, Alonso JR, Lledó PM, Weruaga E (2012) Bone marrow cell transplantation restores olfaction in the degenerated olfactory bulb. *J Neurosci* 32(26):9053–9058. doi:[10.1523/JNEUROSCI.0260-12.2012](https://doi.org/10.1523/JNEUROSCI.0260-12.2012)
- Dodé C, Hardelin JP (2009) Kallmann syndrome. *Eur J Hum Genet* 17(2):139–146. doi:[10.1038/ejhg.2008.206](https://doi.org/10.1038/ejhg.2008.206)
- Dodé C, Levilliers J, Dupont JM, De Paepe A, Le Du N, Soussi-Yanicostas N, Coimbra RS, Delmaghani S, Compain-Nouaille S, Baverel F, Pecheux C, Le Tessier D, Cruaud C, Delpech M, Speleman F, Vermeulen S, Amalfitano A, Bachelot Y, Bouchard P, Cabrol S, Carel JC, Delemarre-van de Waal H, Goulet-Salmon B, Kottler ML, Richard O, Sanchez-Franco F, Saura R, Young J, Petit C, Hardelin JP (2003) Loss-of-function mutations in FGFR1 cause autosomal dominant Kallmann syndrome. *Nat Genet* 33(4):463–465. doi:[10.1038/ng1122](https://doi.org/10.1038/ng1122)
- Doetsch F, Caille I, Lim DA, García-Verdugo JM, Álvarez-Buylla A (1999) Subventricular zone astrocytes are neural stem cells in the adult mammalian brain. *Cell* 97(6):703–716 pii: S0092-8674(00)80783-7
- Doetsch F, Petreanu L, Caille I, García-Verdugo JM, Álvarez-Buylla A (2002) EGF converts transit-amplifying neurogenic precursors in the adult brain into multipotent stem cells. *Neuron* 36(6):1021–1034 pii: S0896627302011339
- Endo Y, Ishiwata-Endo H, Yamada KM (2012) Extracellular matrix protein anosmin promotes neural crest formation and regulates FGF, BMP, and WNT activities. *Dev Cell* 23(2):305–316. doi:[10.1016/j.devcel.2012.07.006](https://doi.org/10.1016/j.devcel.2012.07.006)
- Esteban PF, Murcia-Belmonte V, García-Gonzalez D, de Castro F (2013) The cysteine-rich region and the whey acidic protein domain are essential for anosmin-1 biological functions. *J Neurochem* 124(5):708–720. doi:[10.1111/jnc.12104](https://doi.org/10.1111/jnc.12104)
- Evans MJ, Fanucchi MV, Van Winkle LS, Baker GL, Murphy AE, Nishio SJ, Sannes PL, Plopper CG (2002) Fibroblast growth factor-2 during postnatal development of the tracheal basement membrane zone. *Am J Physiol Lung Cell Mol Physiol* 283(6):L1263–L1270. doi:[10.1152/ajplung.00180.2002](https://doi.org/10.1152/ajplung.00180.2002)

- Franco B, Guioli S, Pragliola A, Incerti B, Bardoni B, Tonlorenzi R, Carozzo R, Maestrini E, Pieretti M, Taillon-Miller P, Brown CJ, Willard HF, Lawrence C, Graziella Persico M, Camerino G, Ballabio A (1991) A gene deleted in Kallmann's syndrome shares homology with neural cell adhesion and axonal path-finding molecules. *Nature* 353(6344):529–536. doi:10.1038/353529a0
- Furusho M, Kaga Y, Ishii A, Hebert JM, Bansal R (2011) Fibroblast growth factor signaling is required for the generation of oligodendrocyte progenitors from the embryonic forebrain. *J Neurosci* 31(13):5055–5066. doi:10.1523/JNEUROSCI.4800-10.2011
- Gálvez-Contreras AY, González-Castañeda RE, Luquín S, González-Pérez O (2012) Role of fibroblast growth factor receptors in astrocytic stem cells. *Curr Signal Transduct Ther* 7(1):81–86. doi:10.2174/157436212799278205
- García-González D, Clemente D, Coelho M, Esteban PF, Soussi-Yanicostas N, de Castro F (2010) Dynamic roles of FGF-2 and anosmin-1 in the migration of neuronal precursors from the subventricular zone during pre- and postnatal development. *Exp Neurol* 222(2):285–295. doi:10.1016/j.expneurol.2010.01.006
- Ghashghaei HT, Lai C, Anton ES (2007) Neuronal migration in the adult brain: are we there yet? *Nat Rev Neurosci* 8(2):141–151. doi:10.1038/nrn2074
- Gianola S, de Castro F, Rossi F (2009) Anosmin-1 stimulates outgrowth and branching of developing Purkinje axons. *Neuroscience* 158(2):570–584. doi:10.1016/j.neuroscience.2008.10.022
- González-Martínez D, Kim SH, Hu Y, Guimond S, Schofield J, Winyard P, Vannelli GB, Turnbull J, Bouloux PM (2004) Anosmin-1 modulates fibroblast growth factor receptor 1 signaling in human gonadotropin-releasing hormone olfactory neuroblasts through a heparan sulfate-dependent mechanism. *J Neurosci* 24(46):10384–10392. doi:10.1523/JNEUROSCI.3400-04.2004
- Gritti A, Frolichsthal-Schoeller P, Galli R, Parati EA, Cova L, Pagano SF, Bjornson CR, Vescovi AL (1999) Epidermal and fibroblast growth factors behave as mitogenic regulators for a single multipotent stem cell-like population from the subventricular region of the adult mouse forebrain. *J Neurosci* 19(9):3287–3297
- Gundersen HJ, Bendtsen TF, Korbo L, Marcussen N, Moller A, Nielsen K, Nyengaard JR, Pakkenberg B, Sorensen FB, Vesterby A et al (1988) Some new, simple and efficient stereological methods and their use in pathological research and diagnosis. *APMIS* 96(5):379–394
- Gunning P, Leavitt J, Muscat G, Ng SY, Kedes L (1987) A human beta-actin expression vector system directs high-level accumulation of antisense transcripts. *Proc Natl Acad Sci USA* 84(14):4831–4835
- Gutiérrez-Mecinas M, Crespo C, Blasco-Ibáñez JM, Gracia-Llanes FJ, Marqués-Marí AI, Nacher J, Varea E, Martínez-Guijarro FJ (2005) Distribution of D2 dopamine receptor in the olfactory glomeruli of the rat olfactory bulb. *Eur J Neurosci* 22(6):1357–1367. doi:10.1111/j.1460-9568.2005.04328.x
- Han YG, Kim HJ, Dlugosz AA, Ellison DW, Gilbertson RJ, Álvarez-Buylla A (2009) Dual and opposing roles of primary cilia in medulloblastoma development. *Nat Med* 15(9):1062–1065. doi:10.1038/nm.2020
- Hawkes C (2003) Olfaction in neurodegenerative disorder. *Mov Disord* 18(4):364–372. doi:10.1002/mds.10379
- Hébert JM, Lin M, Partanen J, Rossant J, McConnell SK (2003) FGF signaling through FGFR1 is required for olfactory bulb morphogenesis. *Development* 130(6):1101–1111
- Hu Y, González-Martínez D, Kim SH, Bouloux PM (2004) Cross-talk of anosmin-1, the protein implicated in X-linked Kallmann's syndrome, with heparan sulphate and urokinase-type plasminogen activator. *Biochem J* 384(Pt 3):495–505. doi:10.1042/BJ20041078
- Hu Y, Guimond SE, Travers P, Cadman S, Hohenester E, Turnbull JE, Kim SH, Bouloux PM (2009) Novel mechanisms of fibroblast growth factor receptor 1 regulation by extracellular matrix protein anosmin-1. *J Biol Chem* 284(43):29905–29920. doi:10.1074/jbc.M109.049155
- Hynes RO (2009) The extracellular matrix: not just pretty fibrils. *Science* 326(5957):1216–1219. doi:10.1126/science.1176009
- Ihrig RA, Álvarez-Buylla A (2011) Lake-front property: a unique germinal niche by the lateral ventricles of the adult brain. *Neuron* 70(4):674–686. doi:10.1016/j.neuron.2011.05.004
- Kallmann F, Schoenfeld W, Barrera S (1944) The genetic aspects of primary eunuchoidism. *Am J Ment Defic* XLVIII:203–236
- Kazanis I, french-Constant C (2011) Extracellular matrix and the neural stem cell niche. *Dev Neurobiol* 71(11):1006–1017. doi:10.1002/dneu.20970
- Kerever A, Schnack J, Vellinga D, Ichikawa N, Moon C, Arikawa-Hirasawa E, Efrid JT, Mercier F (2007) Novel extracellular matrix structures in the neural stem cell niche capture the neurogenic factor fibroblast growth factor 2 from the extracellular milieu. *Stem Cells* 25(9):2146–2157. doi:10.1634/stemcells.2007-0082
- Khodosevich K, Lazarini F, von Engelhardt J, Kaneko H, Lledo PM, Monyer H (2013) Connective tissue growth factor regulates interneuron survival and information processing in the olfactory bulb. *Neuron* 79(6):1136–1151. doi:10.1016/j.neuron.2013.07.011
- Klejbor I, Myers JM, Hausknecht K, Corso TD, Gambino AS, Morys J, Maher PA, Hard R, Richards J, Stachowiak EK, Stachowiak MK (2006) Fibroblast growth factor receptor signaling affects development and function of dopamine neurons—inhibition results in a schizophrenia-like syndrome in transgenic mice. *J Neurochem* 97(5):1243–1258. doi:10.1111/j.1471-4159.2006.03754.x
- Kohwi M, Petryniak MA, Long JE, Ekker M, Obata K, Yanagawa Y, Rubenstein JL, Alvarez-Buylla A (2007) A subpopulation of olfactory bulb GABAergic interneurons is derived from Emx1- and Dlx5/6-expressing progenitors. *J Neurosci* 27(26):6878–6891. doi:10.1523/JNEUROSCI.0254-07.2007
- Kokovay E, Goderie S, Wang Y, Lotz S, Lin G, Sun Y, Roysam B, Shen Q, Temple S (2010) Adult SVZ lineage cells home to and leave the vascular niche via differential responses to SDF1/CXCR4 signaling. *Cell Stem Cell* 7(2):163–173. doi:10.1016/j.stem.2010.05.019
- Kosaka K, Kosaka T (2005) Synaptic organization of the glomerulus in the main olfactory bulb: compartments of the glomerulus and heterogeneity of the periglomerular cells. *Anat Sci Int* 80(2):80–90. doi:10.1111/j.1447-073x.2005.00092.x
- Kovacs T (2004) Mechanisms of olfactory dysfunction in aging and neurodegenerative disorders. *Ageing Res Rev* 3(2):215–232. doi:10.1016/j.arr.2003.10.003
- Lazarini F, Lledó PM (2011) Is adult neurogenesis essential for olfaction? *Trends Neurosci* 34(1):20–30. doi:10.1016/j.tins.2010.09.006
- Lazarini F, Mouthon MA, Gheusi G, de Chaumont F, Olivo-Marín JC, Lamarque S, Abrous DN, Boussin FD, Lledó PM (2009) Cellular and behavioral effects of cranial irradiation of the subventricular zone in adult mice. *PLoS ONE* 4(9):e7017. doi:10.1371/journal.pone.0007017
- Legouis R, Hardelin JP, Levilliers J, Claverie JM, Compain S, Wunderle V, Millasseau P, Le Paslier D, Cohen D, Caterina D et al (1991) The candidate gene for the X-linked Kallmann syndrome encodes a protein related to adhesion molecules. *Cell* 67(2):423–435 pii: 0092-8674(91)90193-3
- Lehtinen MK, Zappaterra MW, Chen X, Yang YJ, Hill AD, Lun M, Maynard T, Gonzalez D, Kim S, Ye P, D'Ercole AJ, Wong ET,

- LaMantia AS, Walsh CA (2011) The cerebrospinal fluid provides a proliferative niche for neural progenitor cells. *Neuron* 69(5):893–905. doi:[10.1016/j.neuron.2011.01.023](https://doi.org/10.1016/j.neuron.2011.01.023)
- Li A, Saito M, Chuang JZ, Tseng YY, Dedesma C, Tomizawa K, Kaitsuka T, Sung CH (2011a) Ciliary transition zone activation of phosphorylated Tctex-1 controls ciliary resorption, S-phase entry and fate of neural progenitors. *Nat Cell Biol* 13(4):402–411. doi:[10.1038/ncb2218](https://doi.org/10.1038/ncb2218)
- Li X, Sun C, Lin C, Ma T, Madhavan MC, Campbell K, Yang Z (2011b) The transcription factor Sp8 is required for the production of parvalbumin-expressing interneurons in the olfactory bulb. *J Neurosci* 31(23):8450–8455. doi:[10.1523/JNEUROSCI.0939-11.2011](https://doi.org/10.1523/JNEUROSCI.0939-11.2011)
- Liberia T, Blasco-Ibáñez JM, Nácher J, Varea E, Lanciego JL, Crespo C (2013) Two types of periglomerular cells in the olfactory bulb of the macaque monkey (*Macaca fascicularis*). *Brain Struct Funct* 218(4):873–887. doi:[10.1007/s00429-012-0435-0](https://doi.org/10.1007/s00429-012-0435-0)
- Lledó PM, Merkle FT, Álvarez-Buylla A (2008) Origin and function of olfactory bulb interneuron diversity. *Trends Neurosci* 31(8):392–400. doi:[10.1016/j.tins.2008.05.006](https://doi.org/10.1016/j.tins.2008.05.006)
- Lois C, Álvarez-Buylla A (1994) Long-distance neuronal migration in the adult mammalian brain. *Science* 264(5162):1145–1148
- Lois C, García-Verdugo JM, Álvarez-Buylla A (1996) Chain migration of neuronal precursors. *Science* 271(5251):978–981
- Luskin MB (1993) Restricted proliferation and migration of postnatally generated neurons derived from the forebrain subventricular zone. *Neuron* 11(1):173–189 pii: 0896-6273(93)90281-U
- Macatee TL, Hammond BP, Arenkiel BR, Francis L, Frank DU, Moon AM (2003) Ablation of specific expression domains reveals discrete functions of ectoderm- and endoderm-derived FGF8 during cardiovascular and pharyngeal development. *Development* 130(25):6361–6374. doi:[10.1242/dev.00850](https://doi.org/10.1242/dev.00850)
- Martín C, Bueno D, Alonso MI, Moro JA, Callejo S, Parada C, Martín P, Carnicero E, Gato A (2006) FGF2 plays a key role in embryonic cerebrospinal fluid trophic properties over chick embryo neuroepithelial stem cells. *Dev Biol* 297(2):402–416. doi:[10.1016/j.ydbio.2006.05.010](https://doi.org/10.1016/j.ydbio.2006.05.010)
- Menn B, García-Verdugo JM, Yachine C, González-Pérez O, Rowitch D, Álvarez-Buylla A (2006) Origin of oligodendrocytes in the subventricular zone of the adult brain. *J Neurosci* 26(30):7907–7918. doi:[10.1523/JNEUROSCI.1299-06.2006](https://doi.org/10.1523/JNEUROSCI.1299-06.2006)
- Mercier F, Kitasako JT, Hatton GI (2002) Anatomy of the brain neurogenic zones revisited: fractones and the fibroblast/macrophage network. *J Comp Neurol* 451(2):170–188. doi:[10.1002/cne.10342](https://doi.org/10.1002/cne.10342)
- Merkle FT, Fuentealba LC, Sanders TA, Magno L, Kessaris N, Álvarez-Buylla A (2014) Adult neural stem cells in distinct microdomains generate previously unknown interneuron types. *Nat Neurosci* 17(2):207–214. doi:[10.1038/nn.3610](https://doi.org/10.1038/nn.3610)
- Mirzadeh Z, Merkle FT, Soriano-Navarro M, García-Verdugo JM, Álvarez-Buylla A (2008) Neural stem cells confer unique pinwheel architecture to the ventricular surface in neurogenic regions of the adult brain. *Cell Stem Cell* 3(3):265–278. doi:[10.1016/j.stem.2008.07.004](https://doi.org/10.1016/j.stem.2008.07.004)
- Mirzadeh Z, Doetsch F, Sawamoto K, Wichterle H, Álvarez-Buylla A (2010a) The subventricular zone en-face: wholemount staining and ependymal flow. *J Vis Exp* (39). doi:[10.3791/1938](https://doi.org/10.3791/1938)
- Mirzadeh Z, Han YG, Soriano-Navarro M, García-Verdugo JM, Álvarez-Buylla A (2010b) Cilia organize ependymal planar polarity. *J Neurosci* 30(7):2600–2610. doi:[10.1523/JNEUROSCI.3744-09.2010](https://doi.org/10.1523/JNEUROSCI.3744-09.2010)
- Mundiñano IC, Caballero MC, Ordóñez C, Hernández M, DiCaulo C, Marcilla I, Erro ME, Tuñón MT, Luquín MR (2011) Increased dopaminergic cells and protein aggregates in the olfactory bulb of patients with neurodegenerative disorders. *Acta Neuropathol* 122(1):61–74. doi:[10.1007/s00401-011-0830-2](https://doi.org/10.1007/s00401-011-0830-2)
- Murcia-Belmonte V, Esteban PF, García-Gonzalez D, de Castro F (2010) Biochemical dissection of Anosmin-1 interaction with FGFR1 and components of the extracellular matrix. *J Neurochem* 115(5):1256–1265. doi:[10.1111/j.1471-4159.2010.07024.x](https://doi.org/10.1111/j.1471-4159.2010.07024.x)
- Murcia-Belmonte V, Medina-Rodríguez EM, Bribián A, de Castro F, Esteban PF (2014) ERK1/2 signaling is essential for the chemoattraction exerted by human FGF2 and human anosmin-1 on newborn rat and mouse OPCs via FGFR1. *Glia*. doi:[10.1002/glia.22609](https://doi.org/10.1002/glia.22609)
- Neugebauer JM, Amack JD, Peterson AG, Bisgrove BW, Yost HJ (2009) FGF signalling during embryo development regulates cilia length in diverse epithelia. *Nature* 458(7238):651–654. doi:[10.1038/nature07753](https://doi.org/10.1038/nature07753)
- Nissant A, Bardy C, Katagiri H, Murray K, Lledó PM (2009) Adult neurogenesis promotes synaptic plasticity in the olfactory bulb. *Nat Neurosci* 12(6):728–730. doi:[10.1038/nn.2298](https://doi.org/10.1038/nn.2298)
- Nusse R (2003) Wnts and Hedgehogs: lipid-modified proteins and similarities in signaling mechanisms at the cell surface. *Development* 130(22):5297–5305. doi:[10.1242/dev.00821](https://doi.org/10.1242/dev.00821)
- Ohkubo Y, Uchida AO, Shin D, Partanen J, Vaccarino FM (2004) Fibroblast growth factor receptor 1 is required for the proliferation of hippocampal progenitor cells and for hippocampal growth in mouse. *J Neurosci* 24(27):6057–6069. doi:[10.1523/JNEUROSCI.1140-04.2004](https://doi.org/10.1523/JNEUROSCI.1140-04.2004)
- Ortega F, Costa MR, Simon-Ebert T, Schroeder T, Gotz M, Berninger B (2011) Using an adherent cell culture of the mouse subependymal zone to study the behavior of adult neural stem cells on a single-cell level. *Nat Protoc* 6(12):1847–1859. doi:[10.1038/nprot.2011.404](https://doi.org/10.1038/nprot.2011.404)
- Parrish-Aungst S, Shipley MT, Erdelyi F, Szabo G, Puche AC (2007) Quantitative analysis of neuronal diversity in the mouse olfactory bulb. *J Comp Neurol* 501(6):825–836. doi:[10.1002/cne.21205](https://doi.org/10.1002/cne.21205)
- Peterson DA (1999) Quantitative histology using confocal microscopy: implementation of unbiased stereology procedures. *Methods* 18(4):493–507. doi:[10.1006/meth.1999.0818](https://doi.org/10.1006/meth.1999.0818)
- Petreanu L, Álvarez-Buylla A (2002) Maturation and death of adult-born olfactory bulb granule neurons: role of olfaction. *J Neurosci* 22(14):6106–6113 pii: 20026588 22/14/6106
- Pignatelli A, Belluzzi O (2010) Neurogenesis in the adult olfactory bulb. In: Menini A (ed) *The Neurobiology of Olfaction*. CRC Press, Boca Raton (FL)
- Pujadas L, Gruart A, Bosch C, Delgado L, Teixeira CM, Rossi D, de Lecea L, Martínez A, Delgado-García JM, Soriano E (2010) Reelin regulates postnatal neurogenesis and enhances spine hypertrophy and long-term potentiation. *J Neurosci* 30(13):4636–4649. doi:[10.1523/JNEUROSCI.5284-09.2010](https://doi.org/10.1523/JNEUROSCI.5284-09.2010)
- Raballo R, Rhee J, Lyn-Cook R, Leckman JF, Schwartz ML, Vaccarino FM (2000) Basic fibroblast growth factor (Fgf2) is necessary for cell proliferation and neurogenesis in the developing cerebral cortex. *J Neurosci* 20(13):5012–5023 pii: 20/13/5012
- Raymond K, Deugnier MA, Faraldo MM, Glukhova MA (2009) Adhesion within the stem cell niches. *Curr Opin Cell Biol* 21(5):623–629. doi:[10.1016/j.ceb.2009.05.004](https://doi.org/10.1016/j.ceb.2009.05.004)
- Rieger MA, Hoppe PS, Smejkal BM, Eitelhuber AC, Schroeder T (2009) Hematopoietic cytokines can instruct lineage choice. *Science* 325(5937):217–218. doi:[10.1126/science.1171461](https://doi.org/10.1126/science.1171461)
- Rugarli EI, Di Schiavi E, Hilliard MA, Arbucci S, Ghezzi C, Faccioli A, Coppola G, Ballabio A, Bazzicalupo P (2002) The Kallmann syndrome gene homolog in *C. elegans* is involved in epidermal morphogenesis and neurite branching. *Development* 129(5):1283–1294
- Shen Q, Wang Y, Kokovay E, Lin G, Chuang SM, Goderie SK, Roysam B, Temple S (2008) Adult SVZ stem cells lie in a vascular niche: a quantitative analysis of niche cell–cell

- interactions. *Cell Stem Cell* 3(3):289–300. doi:[10.1016/j.stem.2008.07.026](https://doi.org/10.1016/j.stem.2008.07.026)
- Shipley MT, Adamek GD (1984) The connections of the mouse olfactory bulb: a study using orthograde and retrograde transport of wheat germ agglutinin conjugated to horseradish peroxidase. *Brain Res Bull* 12(6):669–688
- Snappyan M, Lemasson M, Brill MS, Blais M, Massouh M, Ninkovic J, Gravel C, Berthod F, Gotz M, Barker PA, Parent A, Saghatelian A (2009) Vasculature guides migrating neuronal precursors in the adult mammalian forebrain via brain-derived neurotrophic factor signaling. *J Neurosci* 29(13):4172–4188. doi:[10.1523/JNEUROSCI.4956-08.2009](https://doi.org/10.1523/JNEUROSCI.4956-08.2009)
- Song C, Leonard BE (2005) The olfactory bulbectomized rat as a model of depression. *Neurosci Biobehav Rev* 29(4–5):627–647. doi:[10.1016/j.neubiorev.2005.03.010](https://doi.org/10.1016/j.neubiorev.2005.03.010)
- Soussi-Yanicostas N, Hardelin JP, Arroyo-Jimenez MM, Ardouin O, Legouis R, Leveilliers J, Traincard F, Betton JM, Cabanié L, Petit C (1996) Initial characterization of anosmin-1, a putative extracellular matrix protein synthesized by definite neuronal cell populations in the central nervous system. *J Cell Sci* 109:1749–1757
- Soussi-Yanicostas N, de Castro F, Julliard AK, Perfettini I, Chedotal A, Petit C (2002) Anosmin-1, defective in the X-linked form of Kallmann syndrome, promotes axonal branch formation from olfactory bulb output neurons. *Cell* 109(2):217–228 pii: S0092867402007134
- Stone DM, Grillo M, Margolis FL, Joh TH, Baker H (1991) Differential effect of functional olfactory bulb deafferentation on tyrosine hydroxylase and glutamic acid decarboxylase messenger RNA levels in rodent juxtglomerular neurons. *J Comp Neurol* 311(2):223–233. doi:[10.1002/cne.903110205](https://doi.org/10.1002/cne.903110205)
- Szabo-Rogers HL, Geetha-Loganathan P, Nimmagadda S, Fu KK, Richman JM (2008) FGF signals from the nasal pit are necessary for normal facial morphogenesis. *Dev Biol* 318(2):289–302. doi:[10.1016/j.ydbio.2008.03.027](https://doi.org/10.1016/j.ydbio.2008.03.027)
- Tavazoie M, Van der Veken L, Silva-Vargas V, Louissaint M, Colonna L, Zaidi B, García-Verdugo JM, Doetsch F (2008) A specialized vascular niche for adult neural stem cells. *Cell Stem Cell* 3(3):279–288. doi:[10.1016/j.stem.2008.07.025](https://doi.org/10.1016/j.stem.2008.07.025)
- Trumpp A, Depew MJ, Rubenstein JL, Bishop JM, Martin GR (1999) Cre-mediated gene inactivation demonstrates that FGF8 is required for cell survival and patterning of the first branchial arch. *Genes Dev* 13(23):3136–3148
- Vaccarino FM, Schwartz ML, Raballo R, Nilsen J, Rhee J, Zhou M, Doetschman T, Coffin JD, Wyland JJ, Hung YT (1999) Changes in cerebral cortex size are governed by fibroblast growth factor during embryogenesis. *Nat Neurosci* 2(3):246–253. doi:[10.1038/6350](https://doi.org/10.1038/6350)
- Wichterle H, Turnbull DH, Nery S, Fishell G, Alvarez-Buylla A (2001) In utero fate mapping reveals distinct migratory pathways and fates of neurons born in the mammalian basal forebrain. *Development* 128(19):3759–3771
- Yanicostas C, Herbomel E, Dipietromaria A, Soussi-Yanicostas N (2009) Anosmin-1a is required for fasciculation and terminal targeting of olfactory sensory neuron axons in the zebrafish olfactory system. *Mol Cell Endocrinol* 312(1–2):53–60. doi:[10.1016/j.mce.2009.04.017](https://doi.org/10.1016/j.mce.2009.04.017)
- Yeh C, Li A, Chuang JZ, Saito M, Caceres A, Sung CH (2013) IGF-1 activates a cilium-localized noncanonical Gbetagamma signaling pathway that regulates cell-cycle progression. *Dev Cell* 26(4):358–368. doi:[10.1016/j.devcel.2013.07.014](https://doi.org/10.1016/j.devcel.2013.07.014)
- Young KM, Fogarty M, Kessaris N, Richardson WD (2007) Subventricular zone stem cells are heterogeneous with respect to their embryonic origins and neurogenic fates in the adult olfactory bulb. *J Neurosci* 27(31):8286–8296. doi:[10.1523/JNEUROSCI.0476-07.2007](https://doi.org/10.1523/JNEUROSCI.0476-07.2007)
- Zaghloul NA, Brugmann SA (2011) The emerging face of primary cilia. *Genesis* 49(4):231–246. doi:[10.1002/dvg.20728](https://doi.org/10.1002/dvg.20728)
- Zheng W, Nowakowski RS, Vaccarino FM (2004) Fibroblast growth factor 2 is required for maintaining the neural stem cell pool in the mouse brain subventricular zone. *Dev Neurosci* 26(2–4):181–196. doi:[10.1159/000082136](https://doi.org/10.1159/000082136)